12-2021

Experimental Study of Progressive Crushing Behaviour in Pultruded E-Glass Tubes Using Crown Triggers and A New Perforated Trigger

Chirag Mohan Dodani

Experimental Study of Progressive Crushing Behaviour in Pultruded E-Glass Tubes Using Crown Triggers and A New Perforated Trigger

by

Chirag Mohan Dodani

Bachelor of Science
Aerospace Engineering
Florida Institute of Technology
2019

A thesis
submitted to the College of Engineering and Science
at Florida Institute of Technology
in partial fulfillment of the requirements
for the degree of

Master of Science
in
Aerospace Engineering

Melbourne, Florida
December, 2021

We the undersigned committee
hereby approve the attached thesis

Experimental Study of Progressive Crushing Behaviour in Pultruded E-Glass Tubes Using Crown Triggers and A New Perforated Trigger by Chirag Mohan Dodani

---

David Fleming, Ph.D.
Associate Professor and Department Head
Aerospace, Physics and Space Sciences

Ronnal Reichard, Ph.D.
Professor
Ocean Engineering and Marine Sciences

Mirmilad Mirsayar, Ph.D.
Assistant Professor
Aerospace, Physics and Space Sciences

Abstract

Title:

Experimental Study of Progressive Crushing Behaviour in Pultruded E-Glass Tubes Using Crown Triggers and A New Perforated Trigger

Author:

Chirag Mohan Dodani

Major Advisor:

David Fleming, Ph.D.

An experimental study is conducted on the progressive crushing behavior and the energy absorption during crushing of pultruded fiberglass tubes, initiated by two types of crush triggers, a previously tested crown trigger, and a new perforated trigger. These crush triggers are introduced at the loading end of a pultruded E-Glass/vinyl-ester, circular tube coupon. Coupons with various trigger diameters and number of holes are crushed under quasi-static compression, to evaluate the trigger effectiveness, crushing response, and energy absorption during sustained crushing. It is observed that all trigger types induced progressive crushing in the splaying mode, characterized by the formation of a debris wedge propagating between the tube wall and a series of fronds or petals on both sides of the tube wall.

In terms of trigger response, crown triggers perform better than perforated triggers as the mean crushing load stabilizes and remains relatively uniform across a large dis-

placement, with some periodic oscillations with a small amplitude. Perforated triggers also induced progressive crushing but at significantly lower loads as compared to crown triggers and with crushing load values oscillating with large amplitudes. A combination of a crown and bevel trigger is the most effective in reducing the initial load spike and maintaining a stable load during crushing. Crown triggers with smaller diameters displayed greater energy absorption than those with larger diameters when Specific Sustained Crushing Stress (SSCS) values are compared.

Table of Contents

List of Figures

List of Tables

Acknowledgements

I would like to thank my advisor, Dr. David Fleming, for introducing me to crashworthy composite structures and for his continued guidance through all years. His knowledge, expertise and welcoming nature helped me develop an interest in composite structures. I would like to thank Dr. Ronnal Reichard for sharing his knowledge of composites, for all the help in making the samples and running the tests, and also for his continued guidance through this study. I would also like to thank my other committee member Dr. Mirmilad Mirsayar for his advice and contribution.

In addition, I would like to thank Prerana for always being there and for the constant support. Finally, I would especially like to thank my parents for supporting me in all my endeavors and believing in me always, without which this would not be possible.

Chapter 1

Introduction

1.1 Composites as energy absorbers

Over the past several decades, extensive research has been conducted on the crashworthiness of automotive and aircraft structures. Crashworthiness is defined as the ability of a vehicle to protect its occupants from injury in the event of a crash. Typically, tubular metallic structures have been used as energy absorbers in the well-known 'crumple-zones' of automotive structures [4]. These structures experience tremendous loads in instances of high-speed impact and the goal is to have these absorbers fail in a stable progressive manner, to help absorb and dissipate the impact energy. The introduction of different material types and manufacturing processes has accelerated the development of effective energy absorbing crash structures. Owing to their high strength and stiffness, low density and reduced part numbers, composite materials are being widely considered for many structural applications [8]. Initial research in the use of composite materials in crashworthy structures began around 1976 [9, 10, 11, 12]. A large number of experimental and theoretical studies [2, 4, 7, 13, 14, 15, 16, 17] have subsequently demonstrated that composite absorbers can have better performance un-

der axial compression as compared to metallic absorbers, as they can absorb more energy per unit mass of material when progressively crushed.

When thin-walled tubular metallic absorbers are loaded in axial compression, they may experience a type of progressive failure where the tube collapses into an accordion shape due to buckling of the tube walls in various buckling modes (Figure 1.1) [1, 2, 18]. This progressive failure folding pattern of metallic crash absorbers leads to oscillations in load values as each fold is flattened out, often with large amplitudes as seen in Figure 1.2. Some research is also conducted by Huang et al. [19] to induce progressive failure in metallic tubes by collapsing tubes in the splitting and curling modes. These failure modes are characterized by the formation of cracks on the four corners of the tube which then propagate down the tube due to continuous tearing. This splits the tube into four free side plates which begin rolling up into curls. Results of this study show that steel and aluminum tubes may have significant energy absorbing capabilities and can exhibit modes of progressive failure, but only after experiencing a large initial load spike. For example in reference [19], tubes typically experienced an initial load spike of approximately 115 kN before rapidly dropping and stabilizing at approximately 30-40 kN during progressive failure. This response is not desirable for an efficient energy absorber. A good energy absorber will initially fail at a load level close to or even smaller than the load required to maintain stable progressive failure.

Well-designed fiber-reinforced composites undergo progressive failure about a nearly constant crush load value with some minor oscillations of a small amplitude (Figure 1.3) [2, 17]. A number of experimental studies have been conducted using various types of composite materials to better understand their energy absorbing capabilities. Materials used in research studies and previous applications range from the most common fiberglass/epoxy [12, 20, 21, 22, 23, 24, 25] and graphite/epoxy laminates [5, 25, 26, 27, 28, 29, 30, 31, 32] to woven jute/epoxy [33], cotton fabric/epoxy [34]

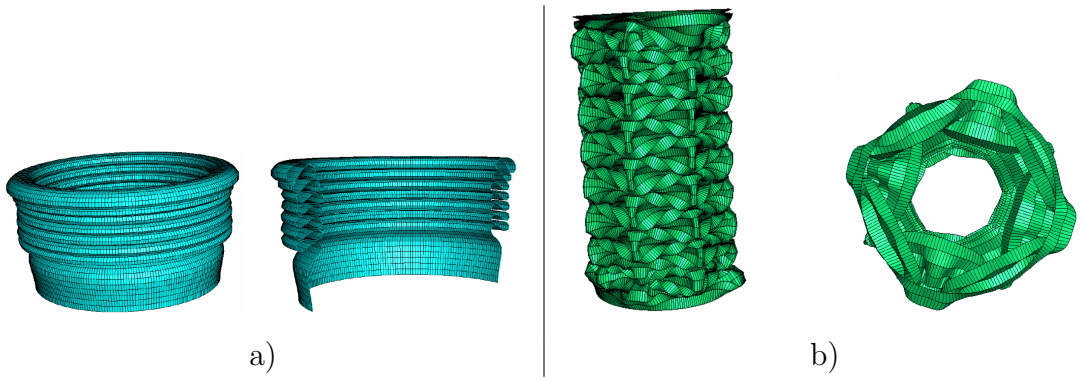

Figure 1.1: a.)Concertina/accordion buckling mode, b.)Diamond 3 lobe mode (from [1])

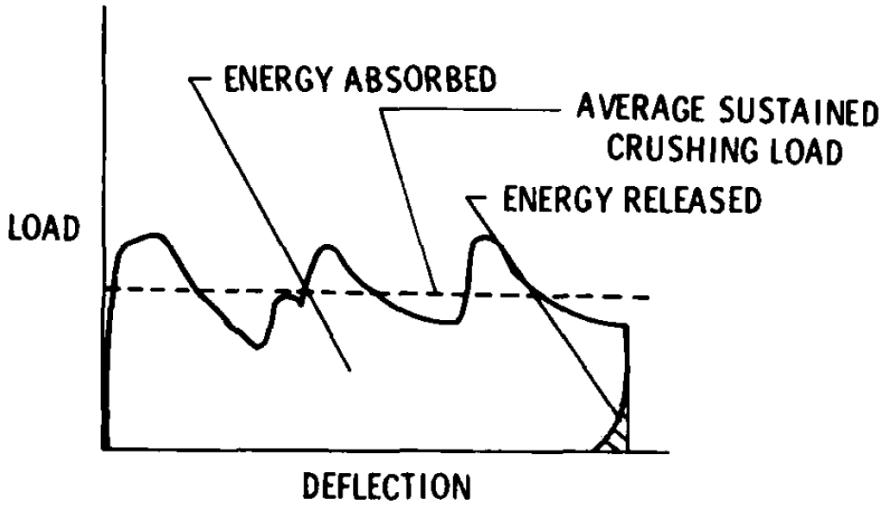

Figure 1.2: Typical load-deflection curve of aluminum tube (from [2])

and even hybrid metal/composite tubes [35, 36, 37].

Most previous studies of composite structures utilize the concept of a trigger in some fashion. Triggers act as initiators of damage and help maintain progressive failure and avoid catastrophic failure due to global buckling or brittle fracture under compression loading. Studies [7, 38, 39, 40, 41, 42, 43] show that numerous parameters influence the crushing response of composite tubes. The energy absorption capability of composites can vary depending on the mechanical properties of the material such as the fiber type,

fiber orientation, fiber and matrix volume fractions, laminate stacking sequence and tube geometry and type of loading, static or dynamic.

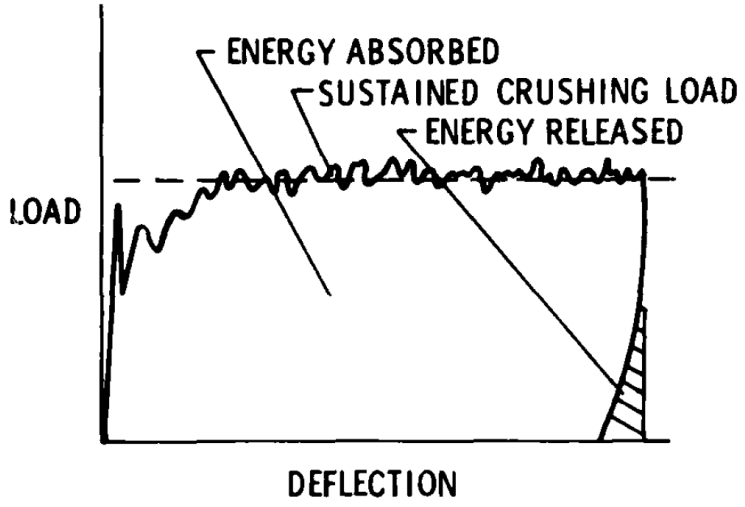

Figure 1.3: Typical load-deflection curve of composite tube (from [2])

There has been a considerable amount of research about which cross-section type is the most efficient in energy absorption. Initially, when energy absorption in composite tubes was being investigated, closed tube specimens with circular or square cross-sections were widely considered due to their simplicity and availability. Early pioneers in this research field, Hull et al. [7], Farley et al. [44] and Thornton et al. [12] all used closed tube circular or square specimens. Studies conducted by Carruthers et al. [15] and Mamalis et al. [29, 42] show that tubes made of the same material with circular cross-sections typically exhibit greater energy absorbing characteristics than square cross-sections. This is mainly due to the stress concentration build-up at the corners of the tubes which may initiate undesirable failure modes. Under axial compression, the corners will begin tearing and the sides will then split after which the tube cannot behave as an effective energy absorber. A variety of other cross-section shapes have been tested. Mamalis et al. [45] also tested glass fiber/vinyl ester tubes with an

hourglass cross-section in the application of automotive frame rails. Results showed that some specimens displayed a stable progressive collapse mode with greater energy absorption as compared to other specimens that experienced axial splits along the curvature change of the specimen. A study conducted by Palanivelu et al. [3] tested nine different geometrical shapes (Figure 1.4) of composite tubes to understand their effect on energy absorption. The study concluded that all cross-sections other than square and hexagonal showed uniform progressive crushing. The square and hexagonal cross-sections however experienced catastrophic failure mainly due to the formation of long axial cracks running along the tube length, originating from the corners. The circular cross-section provided the greatest Specific Energy Absorption (SEA) in all specimens, while the hourglass type – X and hourglass type – Y providing the lowest SEA values due to the absence of circumferential delamination. Hence, based on an extensive literature search, common design principles and material availability, this study solely focuses on altering the trigger parameters of circular cross-section coupons, to study their effect on the progressive crushing response and the energy absorption capability.

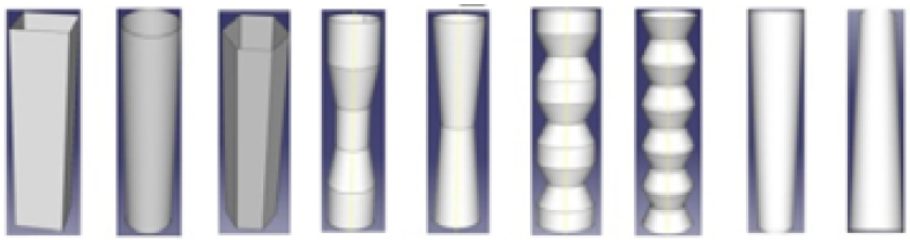

Figure 1.4: Different cross-section tubes tested by Palanivelu et al. (from [3])

1.2 Triggers

Triggers are special modifications made to crash absorbers to help initiate stable crushing at one end of the absorber. These triggers help initiate crack formation and this

"stable zone of microfracture then propagates down the tube" [7]. This helps maintain a nearly constant load level during crushing. Without the use of triggers, these tubes do not behave as energy absorbers. When loaded in axial compression, tubes without a trigger typically experience a large load spike, typically going up to the brittle fracture strength σ_c of the material [7], before the tube catastrophically fails and can no longer maintain its structural integrity. For this reason, the use of triggers is a common practice in the design of composite energy absorbers. Fleming et al. [4] classify triggers into two general classes, internal and external triggers. Any modifications made to the energy absorbers themselves, such as beveled edges or chamfers [12, 20, 21, 22, 23, 24, 27, 30, 33], holes [5, 26] or any cuts [3, 19] etc., that help initially weaken the material at one end to induce crushing, are considered as internal triggers (Figure 1.5) [28, 31, 46]. External triggers are modifications made to the loading structure that makes contact with the absorbers, or any other external means of pre-stressing the absorber on one end, such as external rounded and chamfered crush caps tested by Tong et al. [32], a knife edge trigger tested by Guillon et al. [47] or a Shape Memory Alloy (SMA) wire coil around one end of the tube, as investigated by Huang et al. [28].

A study conducted by Czaplicki et al. [20] used samples of pultruded E-glass/polyester and E-glass/vinyl-ester square tubes with two types of internal triggers, bevel and tulip triggers (Figure 1.5). The samples tested were 150 mm (6 in) long with a fiber volume fraction of 0.52. Results show that the tulip trigger significantly outperformed the bevel trigger with up to two times more energy absorption per unit weight. The tulip trigger also helped maintain a stable progressive crush more efficiently. Another significant observation made is the difference in the load vs. displacement curves. For the bevel trigger, the samples experience an initial load spike after which the load suddenly dropped before rising back up and stabilizing. The tulip trigger samples however

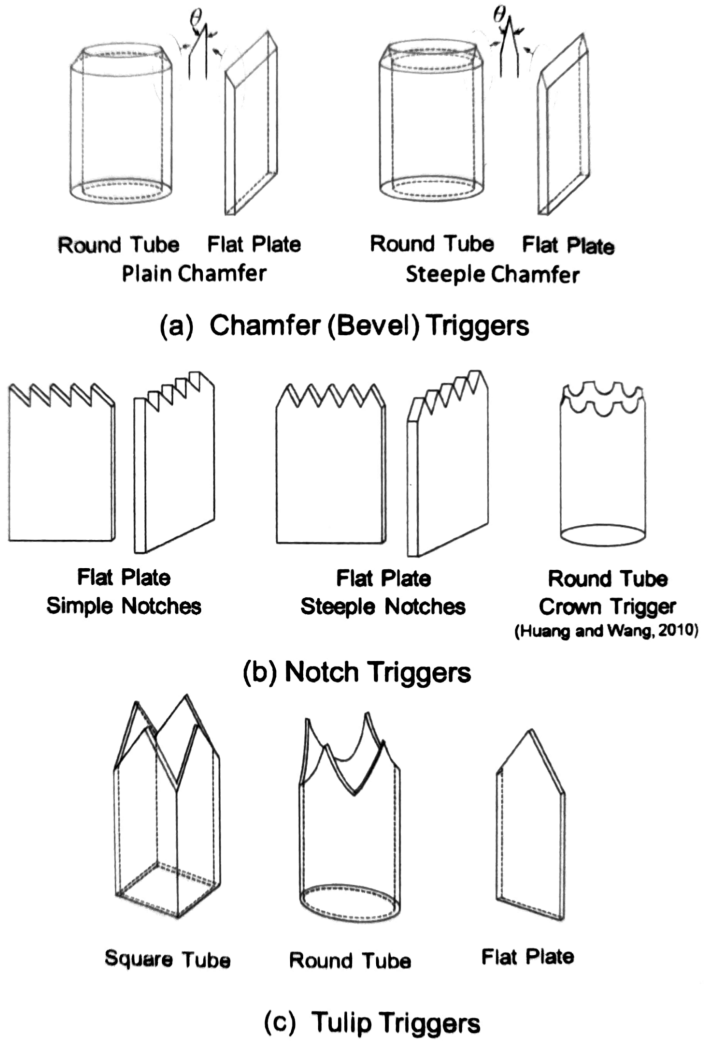

Figure 1.5: Examples of internal triggers (from [4])

experienced an initial load spike after which the load remains relatively stable with minor oscillations, hence having greater energy absorption capability.

Sigalas et el. [22] focused their study solely on the effect of chamfer angles on the crushing response. Fiberglass cloth/epoxy circular tubes were used with chamfer angles ranging from 10° to 90°. The samples tested were 50 mm (1.968 in) long (excluding the chamfer region), 2.5 mm (0.098 in) thick with an outer diameter of 55 mm (2.165 in) and a fiber volume fraction of 0.42. It was found that the chamfer angle greatly

influenced the crushing response. For small chamfer angles of 10° or 20°, the load gradually increases as the crushing zone advances until it stabilizes and progressive crushing continues. Damage is initiated due to the formation of small internal cracks and rings of material resulting from bending fibers. For chamfer angles ranging from 30° to 90°, the load increased almost linearly for a small displacement after which a small load drop occurred, which is associated with the formation of the debris wedge, which will be discussed in the next section. The load then rises back up and stabilizes during progressive crushing. Damage is initiated due to the formation of a long circumferential crack near the loading end. For extreme chamfer angles like 80°, the response resembles that of lower angles but with a significantly greater load drop. From the tests conducted, the small chamfer angles displayed the best response for an efficient energy absorber.

Recently, Huang et al. [5] introduced a new type of internal trigger called a crown trigger at one end of Carbon Fiber Reinforced Polymer (CFRP) circular tubes. The samples tested were made of 14 plies of T700 carbon fiber with BMI resin QY8911 and were 100 mm (3.937 in) long, approximately 1.85 mm (0.072 in) thick with an inside diameter of 50 mm (1.968 in). The crown triggers were comprised of "eight evenly distributed semicircular holes with a radius of 5 mm and a 45°external chamfer" (Figure 1.6). Other trigger types also tested were modifications of the bevel and tulip trigger. Primary parameters evaluated in this study were SEA, Specific Triggering Stress (STS), representing the maximum SEA following which the crush zone is completely formed and the Crush Load Efficiency (CLE) which is a ratio of the SEA to the STS. Quasi-static compression tests performed showed all samples experienced stable progressive crushing with a brittle fracturing crushing mode, as defined by Farley et al. [Farley 1992]. The tube wall was seen to split into three parts, the interior, middle and exterior layers. The failure mode with the crown trigger also showed a large number of shorter

lamina bundles as compared to the failure mode with the bevel trigger. Overall, results show that the new crown trigger performed significantly better than the bevel trigger with nearly the same specific energy absorption but with 18.4% lower STS and 21.2% higher CLE. This implies that the crown triggers can effectively help reduce the impact load felt by occupants of the vehicle, due to its ability to initiate and maintain stable progressive failure.

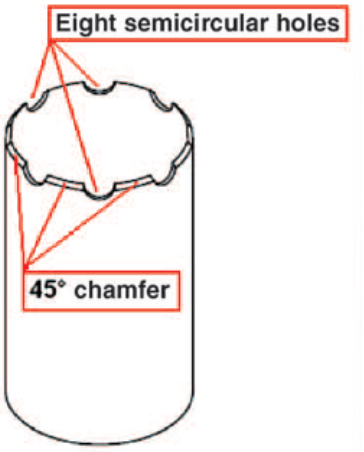

Figure 1.6: Crown trigger introduced by Huang et al. (from [5])

Another study conducted recently by Huang et al. [28] compares the effects of an internal ply drop-off trigger and an external trigger type using a coil of SMA wire around one end of CFRP tubes. The samples tested were made of 12 plies of T700 carbon fiber with BMI resin QY8911 and were 40 mm (1.574 in) long, 3 mm (0.1181 in) thick with an outside diameter of 23 mm (0.905 in) and a fiber volume fraction of 0.64. For the internal ply drop-off trigger, the outer three plies of the specimens were made 4mm shorter than the other plies. For the external SMA trigger, a TiNi (atomic percent Ni = 57.34%) wire with a diameter of 0.5 mm, which was already activated by placing into boiling water for 1 min, was wound around one end of the tube. Results of the study showed that both trigger types can induce stable progressive crushing in the

tubes and increase the SEA and CLE of the tubes. However, the external SMA trigger outperformed the internal ply drop-off trigger with 22.8% higher SEA and 4.3% higher CLE. In addition, this significant improvement is achieved with very little increase of the initial peak crushing stress.

Focusing on pultruded composite tubes, Palanivelu et al. [21] studied the progressive crushing behavior of uni-directional pultruded glass–polyester and glass–vinyl-ester, square and circular tubes subjected to axial impact loading. Samples were tested with either a 45°chamfer or a version of the tulip trigger. The pultruded tube used were made with continuous 0°orientation fibers with random chopped mat on both sides, with a fiber volume fraction of approximately 0.50. Results showed that in terms of energy absorption capability, the chamfer trigger performed better with circular cross-section tubes whereas the tulip trigger performed better with square cross-section tubes. Overall, the circular tubes had a higher SEA value than square tubes. Comparing the effect of the matrix, tubes made of glass vinyl-ester absorbed 33–27% more energy than the glass–polyester tubes. Thornton [46] also studied the crush response of pultruded glass fiber reinforced plastic tubes with a bevel or a tulip trigger, made with either polyester or vinyl-ester resin. Results of this study show that the tulip trigger typically outperformed the bevel trigger when comparing SEA values.

1.3 Progressive crushing of composites

It is evident from the literature, that trigger mechanisms have a significant impact on the progressive crushing response of composite tubes. However, it is also essential to understand how the damage initiated by these triggers propagates through the tube and how this contributes to the overall energy absorption capability. Several different researchers have identified various modes of progressive crushing. Early pioneers of

research in this field, Farley and Jones [44], and Hull [7] were the first to categorize the most common progressive crushing modes in composites.

Farley and Jones [44] used the following three crushing modes to describe progressive crushing of composites:

- Transverse Shearing Crushing Mode (Figure 1.7):

  This crushing mode is characterized by the formation of one or multiple short interlaminar and longitudinal cracks with a relatively small length, typically less than the laminate thickness. This results in the formation of lamina bundles comprised of single or multiple laminae. When further loaded, these interlaminar cracks cause shear failures occurring on principle shear planes of the laminate, resulting in the formation of a sharpened chisel shape. The two crushing mechanisms that control the crushing process in this mode are the interlaminar crack growth and the lamina bundle fracture. The interlaminar crack growth depends on various factors such as mechanical properties of the fiber and fiber orientation. The fracture of lamina bundles however, is the major contributing mechanism in the energy absorption process.

- Lamina Bending Failure Mode (Figure 1.8):

  This crushing mode is characterized by the formation of very long interlaminar and intralaminar cracks as well as long cracks parallel to the fibers with the crack length exceeding the laminate thickness. This results in the formation of bundles that separate from the main laminate on either side of the wall. These bundles exhibit significant bending but do not fracture. The principal mechanism that controls the energy absorption in this mode is matrix crack growth. Other mechanisms affecting this mode are the interlaminar and intralaminar crack growth and friction between adjacent lamina bundles and the friction between the composite

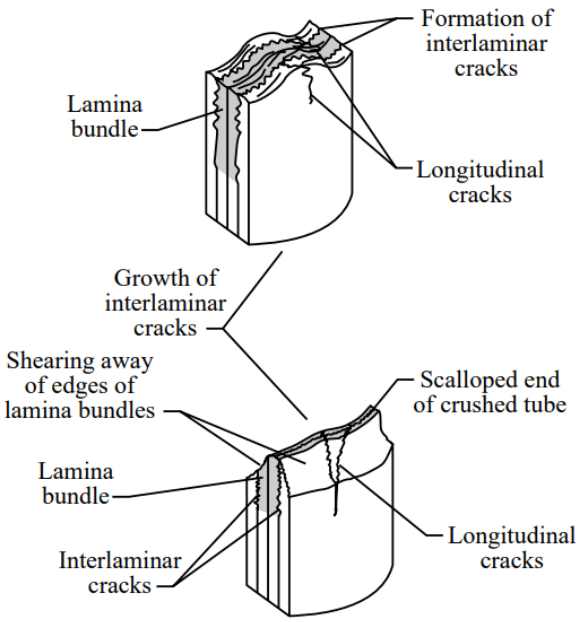

Figure 1.7: Schematic representation of the Transverse Shearing Crushing mode (from [6])

and the crushing surface.

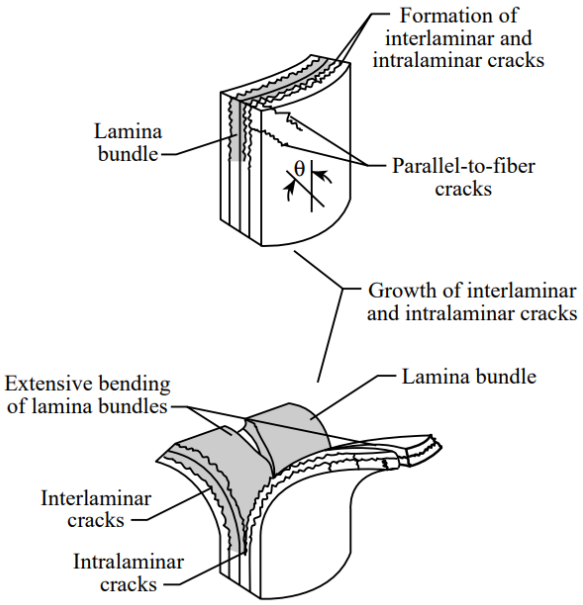

Figure 1.8: Schematic representation of the Lamina Bending mode (from [6])

- Local Buckling Crushing Mode (Figure 1.9):

  This crushing mode is similar to that experienced by ductile materials and is characterized by the formation of interlaminar cracks at buckle zones that lead to the fibers and/or matrix yielding to the stresses. The two crushing mechanisms that control the crushing process in this mode are the plastic yielding of the fiber and/or the matrix. Brittle FRP materials will display this crushing mode only if the strength of the matrix is significantly greater than the interlaminar stresses, the fiber has a lower strain rate than the matrix and the matrix exhibits plastic deformation under high stress values.

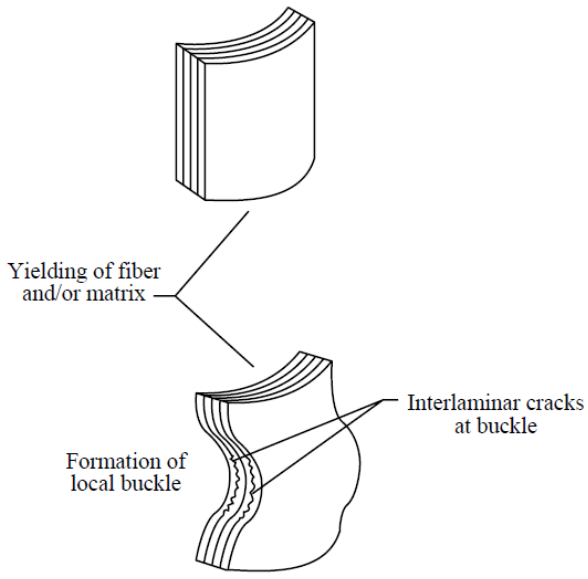

Figure 1.9: Schematic representation of the Local Buckling Crushing mode (from [6])

Hull [7] describes the progressive failure of composites using two categories, namely Progressive Folding and Progressive Crushing, which have since been commonly used by various researchers in their studies.

- Progressive Folding mode:

  This failure mode described by Hull is the same as the Local Buckling Crush-

ing Mode described earlier by Farley and Jones [44]. For this mode, the load-displacement curve can be divided into three distinct sections (Figures 1.10 and 1.11). The initial section is where the sample experiences a rapid load spike up to a maximum value before suddenly dropping. This load drop is associated with the buckling of the folded region that is initiated at one end of the tube and results in the formation of the first complete fold. In the second section, when further loaded, the tube undergoes progressive failure as the load oscillates about an average value while the folds continue to form and propagate down the tube. The last and final region begins at the point when the tube is fully folded and the load recorded starts increasing rapidly due to material compaction.

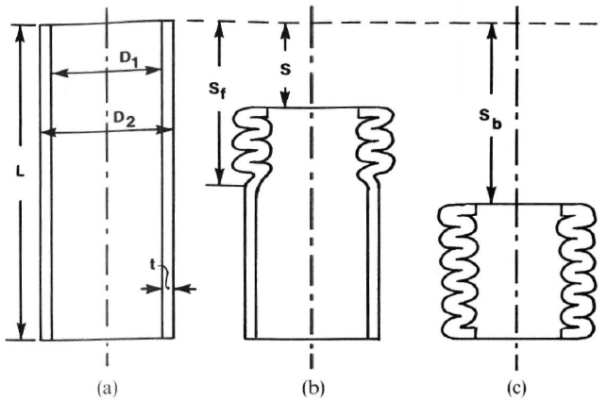

Figure 1.10: Schematic representation of Progressive Folding mode (from [7])

- Progressive Crushing mode:

  In this failure mode, the sample initially experiences a large load spike, typically going up to the brittle fracture strength of the material. At this point, local fracture occurs at the triggers and a sharp load drop is visible after which the load stabilizes and a crush zone is formed (Figures 1.12 and 1.13). Upon further loading, this crush zone propagates down the tube at a nearly constant load level with minor oscillations, making a serrated pattern on the load vs. displacement

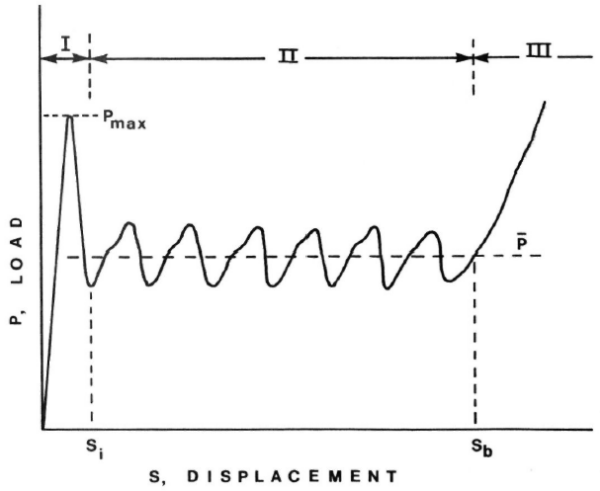

Figure 1.11: Typical load displacement curve for Progressive Folding mode (from [7])

curve. This serrated pattern is distinctive of the progressive crushing mode. Looking closely at the serrated pattern of the load vs. displacement curve during progressive crushing (Figure 1.14), point B corresponds to the load value for crack formation. The slope of line AB depends upon the geometry and stiffness of the tube. At point B, the crack is initiated which then continues to propagate down the tube until point C, where the load is not sufficient for further crack propagation. The load then rises back to that for crack formation, and this sequence repeats itself until all the material has been crushed and a large load spike is visible due to material compaction.

The Progressive Crushing mode is further divided into two categories:

- Fragmentation Mode: This mode is characterized by the progressive formation of a large number of small fragments due to shear failures on both sides of the tube wall resulting from cracks parallel to the fibers (Figure 1.15).
- Splaying Mode: This mode is characterized by the formation of a series of fronds on the outside and inside of the tube wall along with the formation

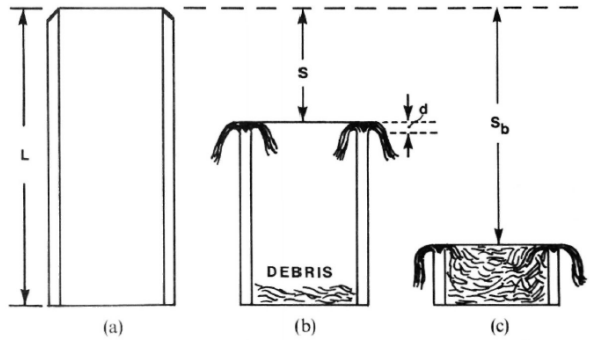

Figure 1.12: Schematic representation of Progressive Crushing mode (from [7])

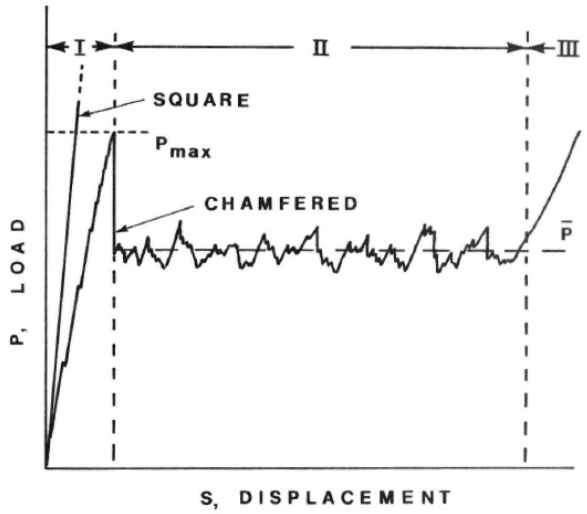

Figure 1.13: Typical load displacement curve for Progressive Crushing mode (from [7])

of a crack along the center of the tube wall. The crushed material forms a wedge of debris at the surface of the crushing platen which splits the tube wall down the middle. (Figure 1.16). As the debris wedge progresses, the axial fibers splay outwards and inwards, the hoop fibers undergo tension and compression respectively and then fracture.

These modes of progressive crushing defined by Farley and Jones [44] and Hull [7] are similar in some ways and generally agree with each other. Studies indicate that composites when crushed will either fail in one of these modes or display a combination

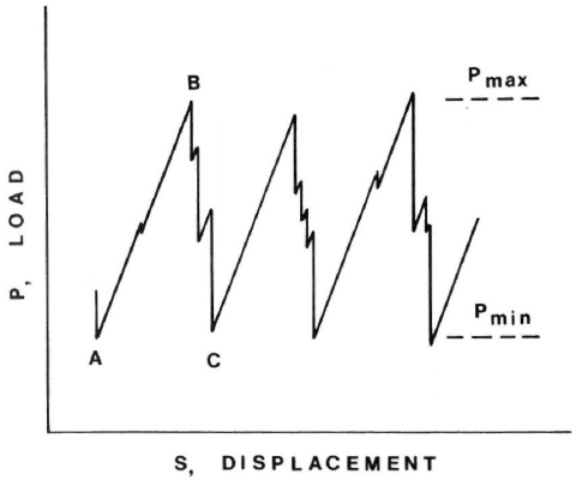

Figure 1.14: Detailed view of the serrated section of the load displacement curve during progressive crushing (from [7])

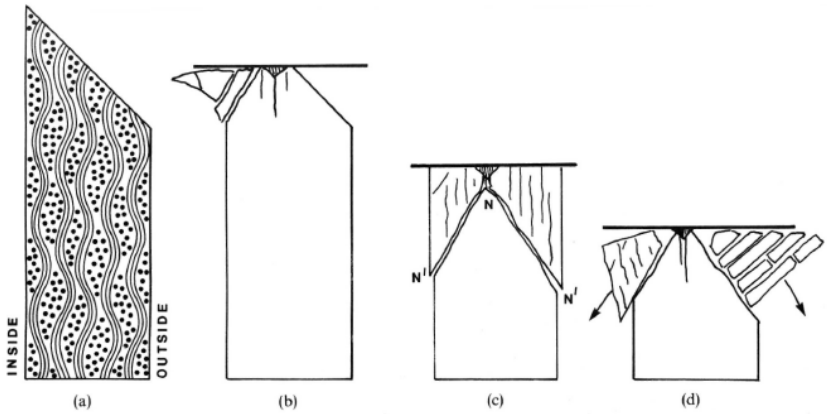

Figure 1.15: Schematic representation of the Fragmentation crushing mode (from [7])

of these modes of failure. Tests conducted in this study use the two modes of progressive crushing defined by Hull [7] to explain the effect of trigger mechanisms on the failure of composite tubes.

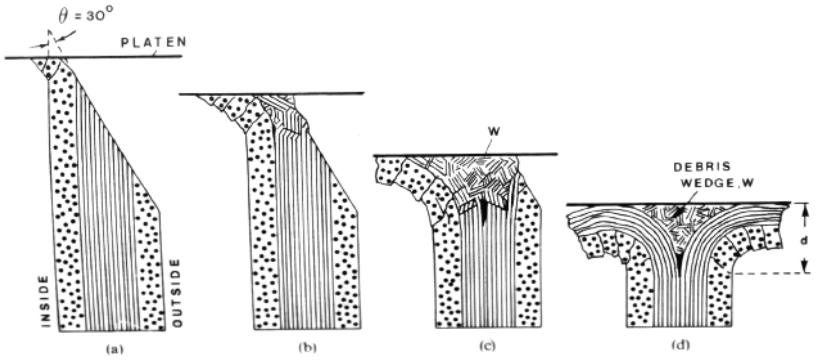

Figure 1.16: Schematic representation of the Splaying crushing mode (from [7])

1.4 Objectives

In this present research, the crown trigger introduced by Huang et al. [5] is further investigated and a new trigger type called perforated trigger is introduced. In addition to triggered samples, one sample is also tested without a trigger for comparative analysis. Diameters and number of crowns and perforations are varied and quasi-static axial compression tests are performed. The primary test parameters evaluated are Specific Sustained Crushing Stress (SSCS) which relates to the energy absorption capability, and the Trigger Ratio (TR) which signifies trigger effectiveness in maintaining progressive crushing. The objectives of this study are to determine if changing the trigger diameters and the number of holes has a significant effect on the SSCS and TR values, and to determine which trigger type or combination of triggers can most effectively reduce the initial load spike experienced by the absorber by initiating damage on one end of the tube, while also maintaining progressive failure in the tube, which helps the overall energy absorption capability. Experimental results are presented, analyzed and discussed, and some conclusions are drawn.

Chapter 2

Experimental Procedure

2.1 Test specimens

All test coupons used were cut from a pultruded circular tube of E-glass/vinyl-ester (VE), manufactured by Strongwell. The material type is identified as EXTREN® 625, a Strongwell VE vinyl-ester resin system with UV inhibitor and flame retardant additives, reinforced with fiberglass. The tube has an outer diameter of 38.10 mm (1.50 in) and a wall thickness of 3.175 mm (1/8 in) with a fiber weight fraction of 54%, matrix weight fraction of 41%, and a 5% weight fraction of additives. The glass fiber reinforcement consists of 50% continuous unidirectional axial fibers with 50% random chopped mat placed on each side of the unidirectional fibers. The layers of randomly oriented fibers help reinforce the tube in directions other than the principal loading direction. These tubes are manufactured using a pultrusion process in which fiberglass tows are pulled through a bath of thermoset resin and then into a heated die for curing. This results in forming structural parts with a high axial strength to weight ratio due to the high fiber content. Table 2.1 provides the mechanical properties of the material used, as provided by Strongwell.

Table 2.1: Material properties of EXTREN® 625 circular tube as provided by Strongwell (LW = Lengthwise, CW = Crosswise)

Property	Units	Value
Density	lbs/in^3	0.062-0.070
	g/cm^3	1.72-1.94
Modulus of Elasticity	10^6 psi	2.8
	10^3 N/mm^2	19.3
Shear Modulus, LW	10^6 psi	0.425
	10^3 N/mm^2	2.93
Poisson Ratio, LW	in/in	0.33
	mm/mm	0.33
Tensile Stress, LW	psi	30,000
	N/mm^2	207
Tensile Stress, CW	psi	7,000
	N/mm^2	48.3
Tensile Modulus, LW	10^6 psi	2.6
	10^3 N/mm^2	17.9
Tensile Modulus, CW	10^6 psi	0.8
	10^3 N/mm^2	5.52
Compressive Stress, LW	psi	30,000
	N/mm^2	207
Compressive Stress, CW	psi	16,000
	N/mm^2	110
Compressive Modulus, LW	10^6 psi	2.6
	10^3 N/mm^2	17.9
Compressive Modulus, CW	10^6 psi	0.8
	10^3 N/mm^2	5.52

The three main trigger types studied are a 45°chamfer, crowns of diameters 1.50 mm (0.06 in), 4.7625 mm (0.19 in) and 9.70 mm (0.38 in), and a new type of perforated trigger with 4.7625 mm (0.19 in) diameter perforations. The chamfer trigger is incorporated into the sample by grinding a 45°chamfer onto the external edge of the tube wall using a belt grinder. The crown trigger is made up of eight evenly spaced semicircular holes drilled into one end of the specimen. The perforated trigger is made up of one or more rows of eight, evenly spaced holes drilled into the tube wall using a bench-top drill press, with each row of perforations spaced 12.7 mm (0.5 in) apart. Overall, seventeen coupons were tested with varying trigger configurations including one coupon with no trigger for a basis of comparison. Some coupons were tested with a single trigger type whereas others were tested with a combination of triggers to evaluate the difference in crushing response, as shown in Table 2.2. Figure 2.1 shows the different types of triggers tested in this study.

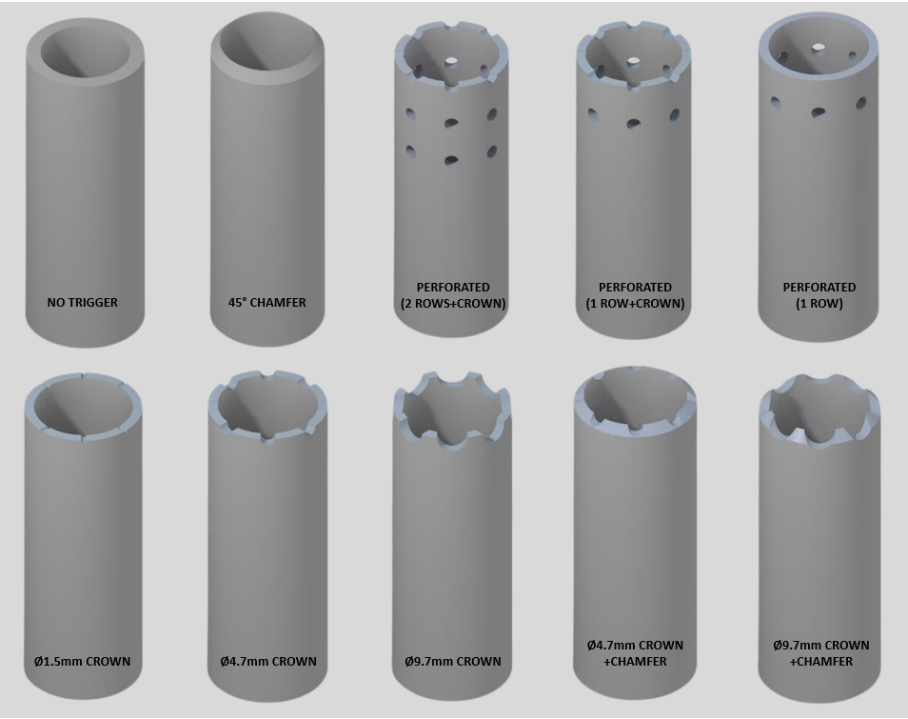

Figure 2.1: Different types of triggers tested

Table 2.2: Specimen details

Sample#	Length(mm)	Trigger type	Diameter (mm)	# of holes
NT1	101.60	No trigger	-	-
BT1	101.60	45°Chamfer	-	-
CT1-1	101.60	Crown	1.5000	8
CT1-2	101.60	Crown	1.5000	8
CT1-3	101.60	Crown	1.5000	16
CT1-4	101.60	Crown	1.5000	16
CT2-1	101.60	Crown	4.7625	8
CT2-2	101.60	Crown	4.7625	8
CT2-3	101.60	Crown+45°chamfer	4.7625	8
CT2-4	101.60	Crown+45°chamfer	4.7625	8
CT3-1	101.60	Crown	9.7000	8
CT3-2	101.60	Crown	9.7000	8
CT3-3	101.60	Crown+45°chamfer	9.7000	8
CT3-4	101.60	Crown+45°chamfer	9.7000	8
PT1-1	101.60	Crown+Perforated (2 rows)	4.7625	24
PT1-2	101.60	Crown+Perforated (1 row)	4.7625	16
PT1-3	101.60	Perforated (1 row)	4.7625	8

2.2 Experimental procedure

All coupons are subjected to quasi-static axial compression tests a room temperature and pressure conditions, using a Tinius Olsen universal testing machine (Figure 2.2) with a max load capacity of 60,000 lbs. All coupons are placed with the edges parallel

to the top and bottom loading platens, with the triggered end of the absorber oriented upwards. The cross-head rate for all tests is set at 1.27 mm/min (0.05 in/min) and all samples are crushed for about 38 mm (1.5 in) length. Load vs. displacement values are recorded and plotted by the DAQ system.

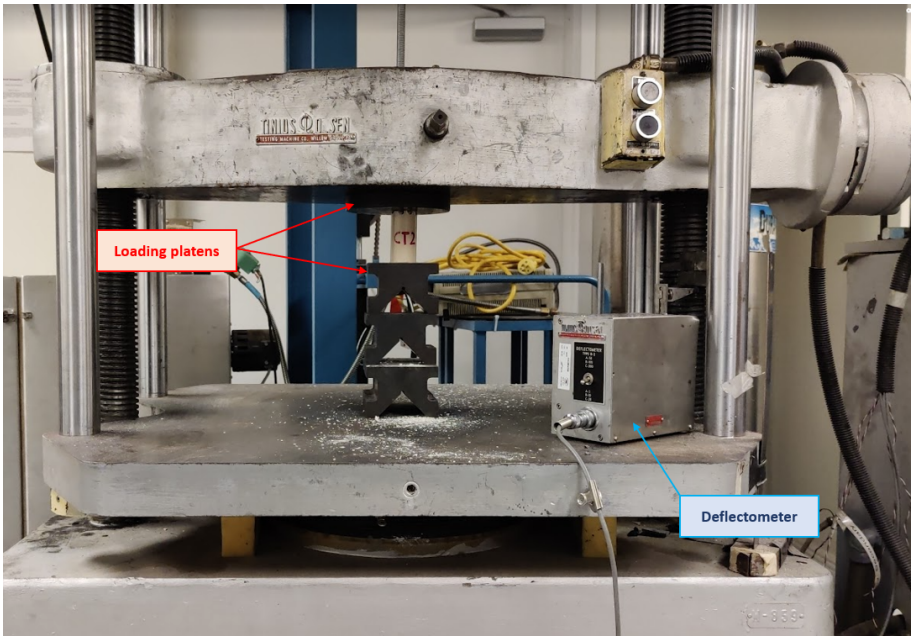

Figure 2.2: Tinius Olsen Universal Testing Machine used for all tests

2.3 Performance Measures

The primary results to be analyzed are Specific Sustained Crushing Stress (SSCS) and Trigger Ratio (TR). Additionally, the maximum triggering load (Pmax) and the average load during sustained crushing (Pm) are also compared to evaluate the trigger response to crushing and the energy absorption capability.

2.3.1 Specific Sustained Crushing Stress (SSCS)

Typically, the Specific Energy Absorption (SEA) of a composite structure is used to describe the amount of energy absorbed per unit mass of the absorber. This is calculated as a ratio of the useful energy absorbed to the total mass of the absorber [48]. This definition of SEA is only applicable when it is applied to the complete absorber. However, many studies conducted show that after the energy absorber is crushed beyond a certain length, a form of material compaction occurs, where all the crushed material compacts into a block of solid material under loading, which results in a significant load spike that may damage the testing equipment. To avoid this, the test is usually stopped at some arbitrary displacement before compaction occurs and the useful energy is computed from zero up to that point of compaction. This practice is widely used in the community for element level testing of energy absorbers. For this study, since the tests do not permit the evaluation of displacement during compaction, an alternate energy absorption parameter, SSCS, is evaluated.

This measure was introduced by Farley et al. [44] and considers the energy absorbed during the sustained crushing part of the response only and neglects the initial elastic and triggering response and the post-compaction response. The sustained crushing part of the response is when the load remains relatively constant with minor oscillations and the crushing mode remains unchanged. Hence, as presented by Fleming and Jackson [4], SSCS can be calculated as,

$$SSCS = \frac{E_{sustained}}{m_{sustained}} \tag{2.1}$$

where $E_{sustained}$ is the energy absorbed during the sustained crushing phase only, represented as,

$$E_{sustained} = \int_{s_i}^{s \leq s_c} F(x)dx \tag{2.2}$$

where s_i is the displacement corresponding to the beginning of sustained crushing and s_c is the displacement corresponding to the end of sustained crushing and the beginning of compaction.

Typically, for a constant geometry specimen like a circula tube, the corresponding mass $m_{sustained}$ is taken as,

$$m_{sustained} = \rho A(s - s_i) \tag{2.3}$$

where ρ is the mass density of the material and A is the uniform cross-section area. Combining equations (2.2) and (2.3) in (2.1) gives,

$$SSCS = \frac{\int_{s_i}^{s \leq s_c} F(x)dx}{\rho A(s - s_i)} \tag{2.4}$$

The mean load P_m experienced during sustained crushing is represented as,

$$P_m = \frac{\int_{s_i}^{s \leq s_c} F(s)dx}{(s - s_i)} \tag{2.5}$$

Substituting eq. (2.5) in eq (2.4) gives us the SSCS in terms of mean load P_m as,

$$SSCS = \frac{P_m}{\rho A} \tag{2.6}$$

Representing this equating in terms of the mean stress during sustained crushing ρ_m,

$$SSCS = \frac{\sigma_m}{\rho} \tag{2.7}$$

This final form of the SSCS equation can be used with the readily available values of density and mean crushing stress to evaluate the energy absorption capability of the absorber. Typical SI units for SSCS or SEA are kJ/kg and Imperial units are lb_f-in/lb_m.

2.3.2 Trigger Ratio (TR)

The trigger ratio is defined as the ratio of the maximum triggering load (P_{max} to the mean load during sustained crushing (P_m). This parameter is also called the Crush Force Efficiency (CFE) by some researchers and can be calculated as,

$$TR = \frac{P_{max}}{P_m} \tag{2.8}$$

The TR is useful in evaluating the effectiveness of the trigger in initiating crushing in the absorber. For an ideal energy absorber, the TR=1. However, for experimental purposes, TR values lower than 1 but closest to 1 are desired. TR values greater than 1 imply that the triggers are not effective in dissipating the energy during initial impact as the maximum triggering load is higher than the mean sustained crushing load.

Chapter 3

Results and Discussion

Force displacement curves for all specimens are shown in Appendix A. These curves also identify the regions of each curve used to define the sustained crushing region, and thus to determine the SSCS. Summary of results for all the specimens with varying trigger types, comparing the SSCS, TR, maximum triggering load P_{max} and the average load during sustained crushing P_m are displayed in Table 3.1. For the samples that experienced catastrophic failure, the maximum triggering value shown in Table 3.1 corresponds to the load value at which failure occurred.

3.1 No Trigger (NT)

When the sample NT1 was loaded under compression, it experienced an initial large load spike up to about 29,800 lbs., after which the sample suffered a catastrophic failure and the load dropped back down to 0 lbs. (Figure 3.1). The primary failure mechanism for this specimen (Figure 3.2) is the inward buckling of the tube wall on the loaded end of the tube. Only one side of the tube experienced this failure as the fibers buckled under compression. The other half of the tube shows some evidence of the beginning

Table 3.1: Summary of results

Specimen ID	SSCS (kJ/kg)	SSCS (kip_f in/lb_m)	TR	P_{max} (kip)	P_m (kip)
NT1	-	-	-	29.81	-
BT1	70.69	283.75	1.01	10.23	10.11
CT1-1	72.63	291.54	1.24	12.92	10.39
CT1-2	73.13	293.53	1.19	12.50	10.46
CT1-3	-	-	-	18.90	-
CT1-4	68.07	273.21	1.22	11.89	9.74
CT2-1	69.43	278.68	0.87	8.68	9.93
CT2-2	76.02	305.14	1.08	11.71	10.87
CT2-3	66.23	265.83	1.06	10.10	9.47
CT2-4	71.48	286.90	1.03	10.55	10.22
CT3-1	67.95	272.77	1.30	12.60	9.72
CT3-2	78.66	315.76	0.83	9.30	11.25
CT3-3	73.12	293.51	1.24	12.98	10.46
CT3-4	72.03	289.14	1.24	12.78	10.30
PT1-1	49.11	197.13	0.89	6.24	7.03
PT1-2	60.58	243.18	0.81	6.99	8.67
PT1-3	-	-	-	16.04	-

of progressive crushing. There is a distinct wedge of debris going through the tube wall, causing the formation of long axial cracks around the circumference. There is also the partial formation of fronds on the inside and outside of the tube wall, which is characteristic of the Splaying Mode of failure (Figure 3.2). However, the sample overall displayed no form of progressive failure and can be used as a basis to compare the effectiveness of the triggers in reducing this initial load spike.

3.2 Chamfer Trigger (BT)

A single specimen with a chamfer trigger was tested, to provide a basis for comparison with the other trigger types that are the primary focus of this study. Stable progressive failure with the Fragmentation Mode and Splaying Mode was observed when the specimen BT1 with the chamfer trigger was crushed. As seen from Figure 3.3, the load

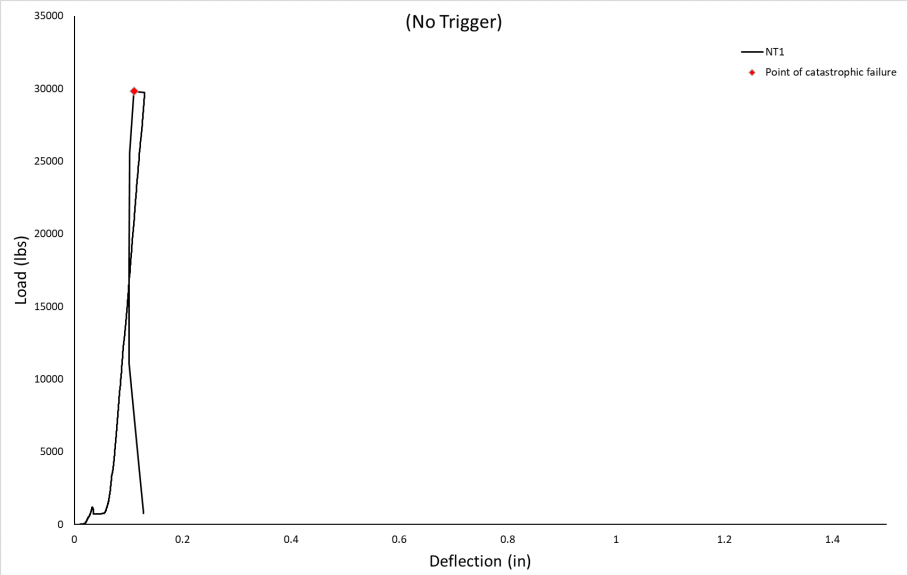

Figure 3.1: Load vs. Displacement curve for sample NT1

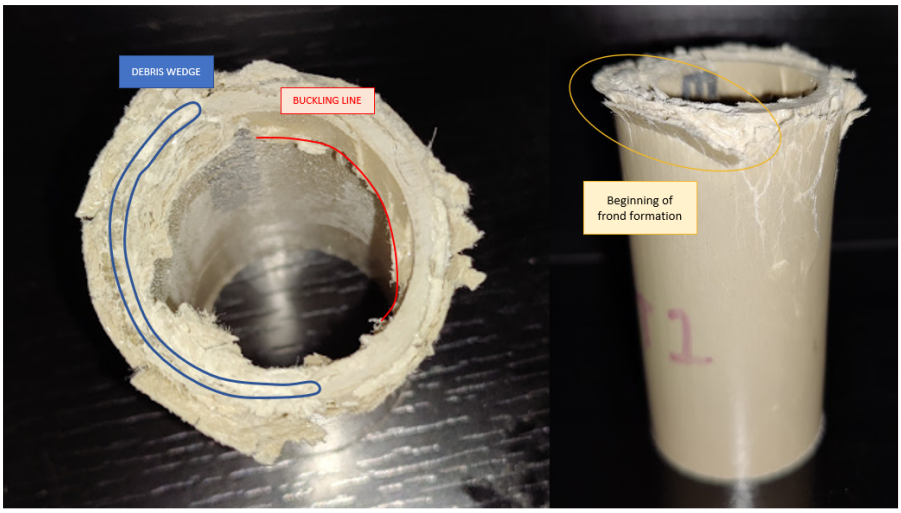

Figure 3.2: Failure mode with no trigger

rises linearly until the first peaks at around 0.24 in and 0.25 in displacement, which is when a large number of transverse cracks originate inside the tube wall (Figure 1.16 (b)) that initiate the transverse shear failure. As loading continues, these transverse cracks continue to propagate until the load peaks again at 10,230 lbs which is the

maximum triggering load. While the load increases, the chamfered edge of the tube is being pulverized and as the walls are shearing away, some debris collects under the platen and forms a wedge that drives through the tube wall. Following this load spike, there is a significant load drop to about 8,000 lbs. which corresponds to the formation of the central wall crack running through the center of the tube wall along with long axial cracks around the circumference of the tube that causes the tube wall to delaminate and buckle. The load then rises back up and stays relatively constant at around 10,100 lbs. with minor oscillations. This is a typical response of progressive crushing in composites where the load required for crack formation is larger than that for crack propagation, giving rise to the corrugated form of the load vs. displacement curve in the sustained crushing region. The specimen with the chamfer trigger has an impressive SSCS value of 70.61 kJ/kg with a TR of 1.01, indicating that it is highly capable of absorbing the initial impact energy and dissipating it. However, a combination of crown and a chamfer displays a higher energy absorption capability with higher sustained crushing loads, as will be seen later. Stable progressive crushing of the specimen led to the formation of long cracks along the length of the tube originating from the crushed end. Initial phases of crushing showed the tube wall split into multiple sections or fronds that began splaying outward, corresponding to the Splaying Mode of crushing. As loading continued, a wedge of debris was formed under that platen that caused the tube wall to split into two layers and the fronds began rolling inwards (Figure 3.4). Approximately seven fronds formed on the outside of the tube wall, which is lower than most other trigger types tested. Overall, the chamfer trigger by itself is an effective energy absorber with the benefit of ease of fabrication.

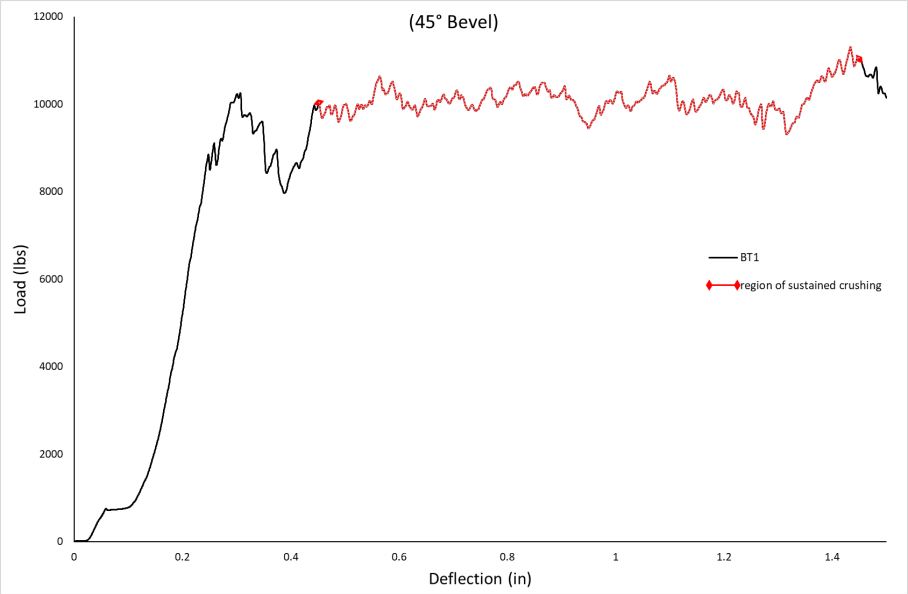

Figure 3.3: Load vs. Displacement curve for sample BT1

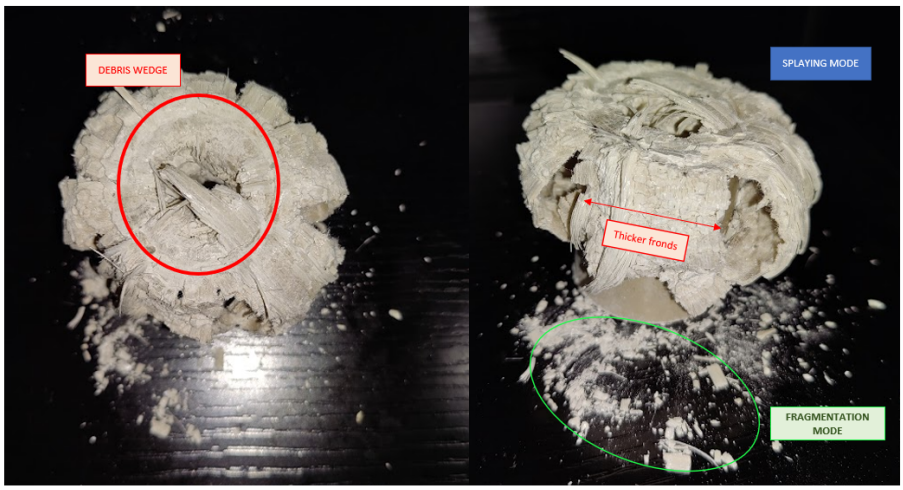

Figure 3.4: Failure mode with chamfer trigger

3.3 Crown Trigger (CT)

Twelve coupons with crown triggers were tested, with three main categories based on the crown diameter; CT1 with 1.5 mm diameter crowns, CT2 with 4.6725 mm diameter crowns and CT3 with 9.7 mm diameter crowns. For samples CT1-1 and CT1-2 with

8 crowns, the typical response (Figure 3.5) was that the load initially rises linearly up to a maximum value, here about 12,500 lbs for both samples, corresponding to the formation of transverse cracks, before the load drops back down to around 10,000 lbs, which is due to the formation of the central wall crack that splits the tube wall into two parts, the interior and exterior layers. Until this point, the sample only displays shear failures in the tube wall and interlaminar cracks that cause small fragments to break off from the tube wall. Once the load is stabilized at around 10,300 lbs – 10,400 lbs, both samples exhibit stable progressive crushing in the Splaying Mode, which occurs due to interlaminar crack growth and fiber tow fracture. As loading progresses, the tube walls continue to fold and roll inwards. The lamina bundles that split away from the tube wall do not experience additional fiber bundle failures. Instead, continued loading initiates long cracks parallel to the fibers which then splits these lamina bundles into two or more sub-laminates which continue to splay outward. CT1-2 has an unusual response with a small load spike at 0.10 in displacement and another significant load spike from 0.30 – 0.40 in displacement, after the formation of the debris wedge. This response can be attributed to the already existing cracks along the tube wall originating from the crown, which occurred during specimen fabrication. Though both CT1-1 and CT1-2 have a high SSCS value 70 kJ/kg, the TR values of 1.24 and 1.19 respectively, suggest that the small diameter crowns are not as efficient in initiating crushing as compared to the chamfered trigger and crowns with larger diameters.

Next, specimens CT1-3 and CT1-4 were tested with the same 1.5 mm diameter crowns but with double, the number of triggers, to compare the effect of the number of triggers on the energy absorption capability and the crushing response. Unfortunately, due to both end surfaces of specimen CT1-3 not being sufficiently parallel as a result of an error in cutting the sample (one end of the tube was slightly longer than the other). When loaded in compression, this specimen experienced catastrophic failure

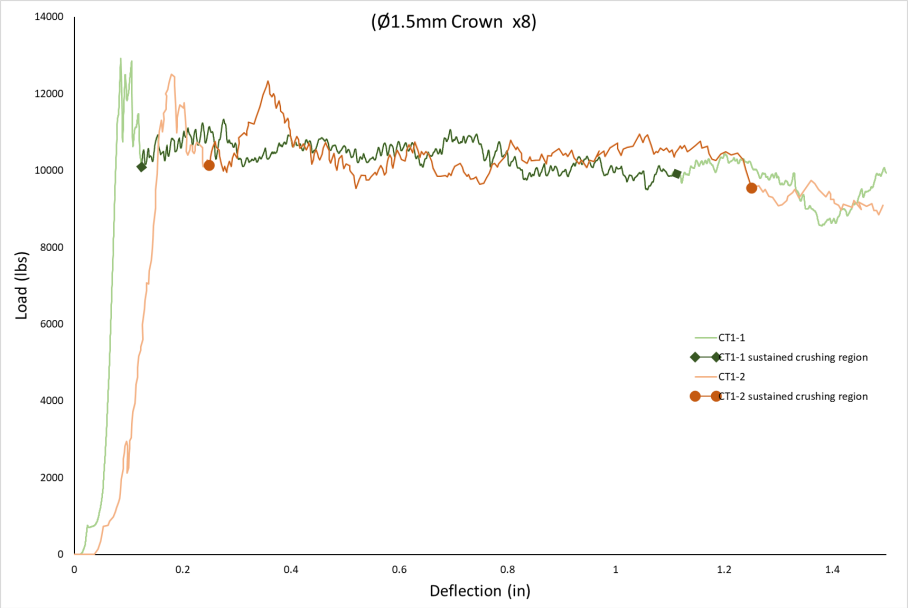

Figure 3.5: Load vs. Displacement curves for samples CT1-1 and CT1-2

due to buckling of the tube wall, as seen in Figure 3.6. Sample CT1-4 however, shows that increasing the number of holes has an adverse effect on the energy absorption capability. As seen in Table 3.1, results show that sample CT1-4 with sixteen holes has about 6% lower SSCS as compared to sample CT1-1 with eight holes. Even though increasing the number of holes helps reduce the maximum triggering load, the loss of energy absorption does not justify the lower load value. Figure 3.7 displays the load vs. displacement curves for both samples CT1-3 and CT1-4.

Crown triggers samples CT2-1 and CT2-2 with a larger crown diameter of 4.7625 mm have better energy absorption capability than samples CT1-1 and CT1-2 with small diameter crowns. As seen from Figure 3.8 and the TR values, there is a noticeable difference in the sustained crushing load value as compared to the maximum triggering value. After the samples experience the final large load spike of the triggering phase and the load drop with the central wall crack formation, the load either rises and stabilizes at a much higher value as seen for CT2-1, or remains at the same value seen for CT2-2.

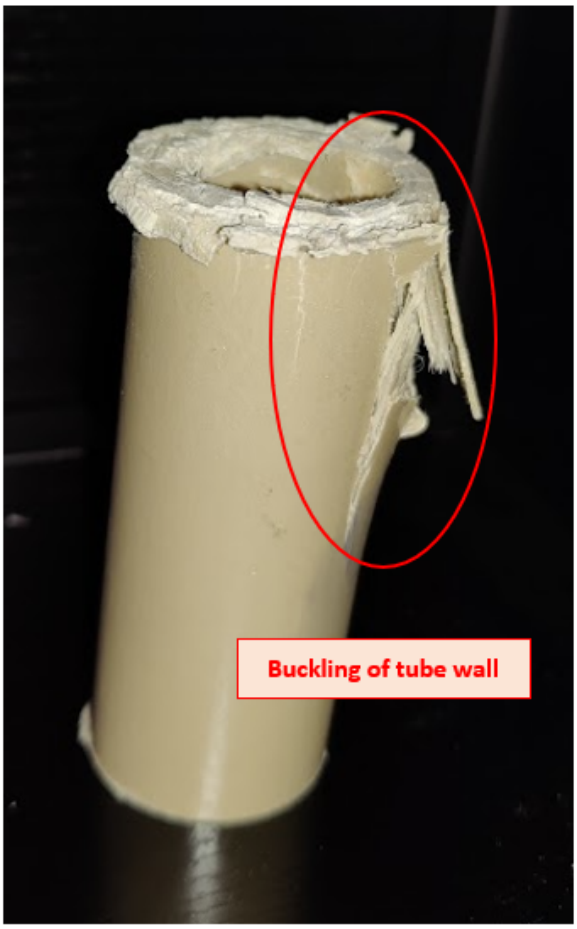

Figure 3.6: Catastrophic failure of sample CT1-3 due to buckling

For samples CT1-1 and CT1-2, the load for sustained crushing is significantly lower than that for triggering. However, there is a large difference in the initial triggering response. As the crowns with larger diameters are initially loaded, the load keeps rising to a maximum value and then suddenly drops significantly. Upon further observation, it was found that this load drop is associated with the formation of interlaminar cracks in the columns of material between the crowns and the formation of the debris wedge which leads to the splitting of the tube wall. Because the height of the columns of material is lower for a smaller diameter, the load drop experienced is smaller.

Even though samples CT2-1 and CT2-2 display good SSCS values, the load drop

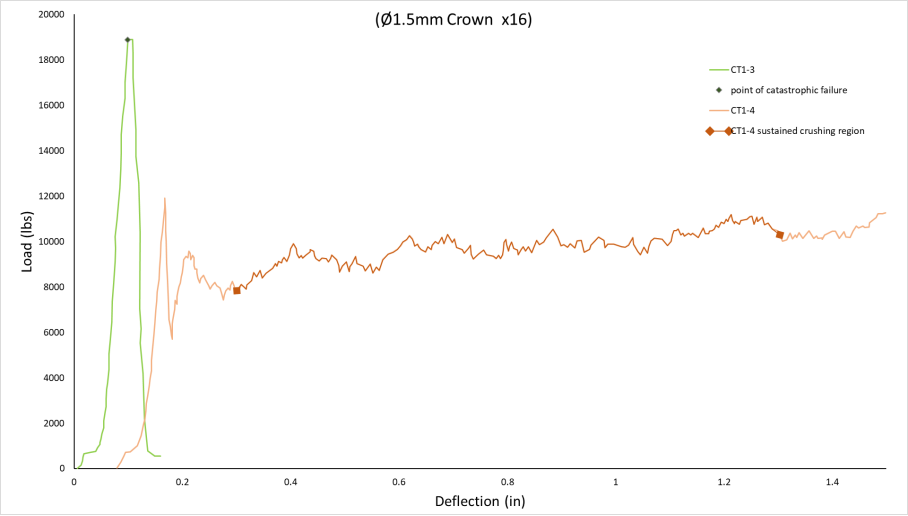

Figure 3.7: Load vs. Displacement curves for samples CT1-3 and CT1-4

discussed earlier is something that should be avoided. To address that, samples CT2-3 and CT2-4 were tested with eight crows in addition to a 45° external chamfer. The decision to incorporate a chamfer was made based on the triggering response observed with sample BT1, with a much smaller load drop. Even though CT2-3 and CT3-4 have similar SSCS values as compared to other samples, the triggering response is significantly better. As seen in Figure 3.9, both samples show a linear increase in the load until the triggering stage, when the first load spikes occur due to the formation of transverse cracks. The response after initial triggering is what makes these triggers one of the best options for energy absorbers. As loading progresses, there is no additional load drop, instead, the load remains relatively uniform with some oscillations. This stable response is attributed to the presence of the chamfer to initiate the formation of the debris wedge. Since the loaded end of the specimen is sharp, damage is initiated with ease and is further assisted by the presence of the crowns.

Finally, samples CT3-1 thru CT-4 were tested with an even larger crown diameter of 9.7mm. Results show that CT3-2 has the highest SSCS value of 78.66 kJ/kg and

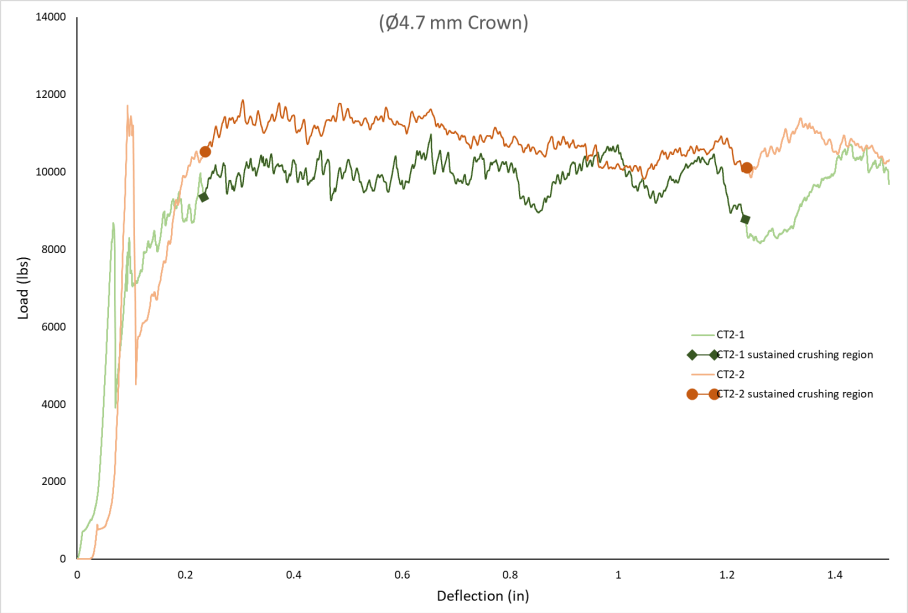

Figure 3.8: Load vs. Displacement curves for samples CT2-1 and CT2-2

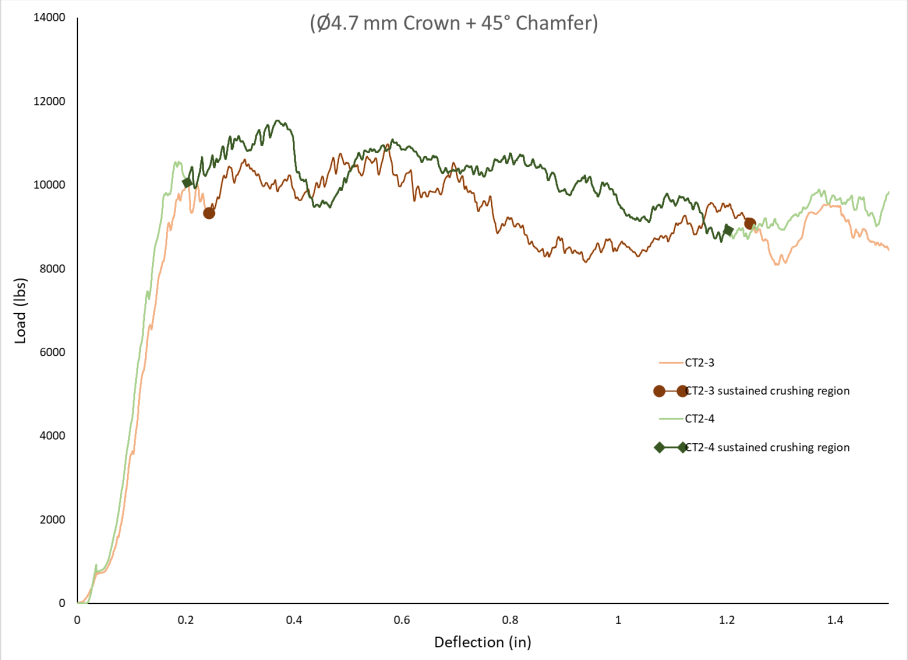

Figure 3.9: Load vs. Displacement curves for samples CT2-3 and CT2-4

one of the best TR values of 0.83, as compared to all other trigger types. This sample performed significantly better than most others as it also has the highest average sustained crushing load and one of the lowest triggering loads, indicating that a larger crown diameter may be more effective in initiating damage in the absorber. Despite the high SSCS value, the initial load drop of about 6000 lbs. is one of the largest seen in all the samples (Figure 3.10). To address this, samples CT3-3 and CT3-4 were tested with an additional 45° external chamfer end of the tube. This addition helps to increase the energy absorption capability, but on the cost of losing trigger effectiveness. When samples with crowns and a chamfer are compared, smaller diameter crowns have a lower SSCS value but exhibit a better triggering response by maintaining the load level after the triggering stage (Figure 3.11).

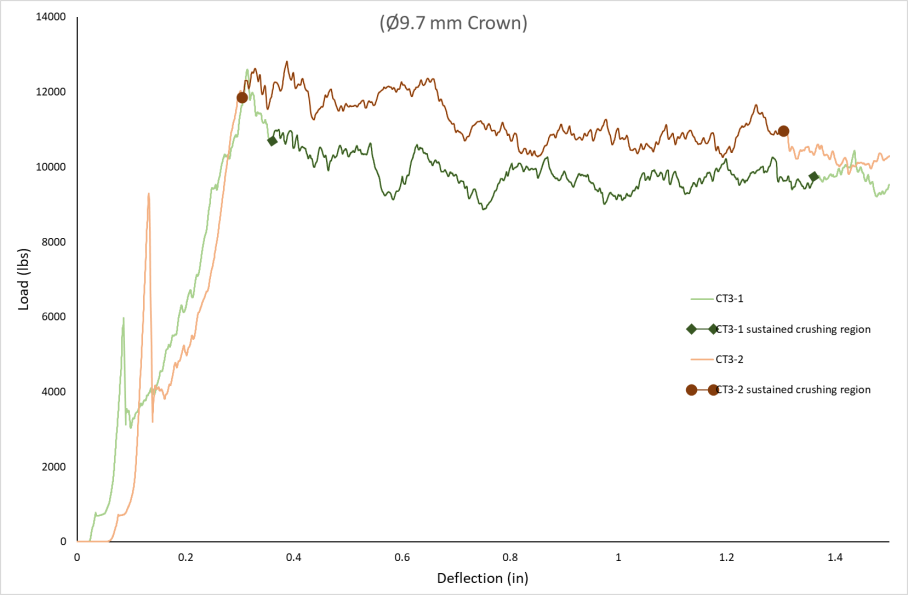

Figure 3.10: Load vs. Displacement curves for samples CT3-1 and CT3-2

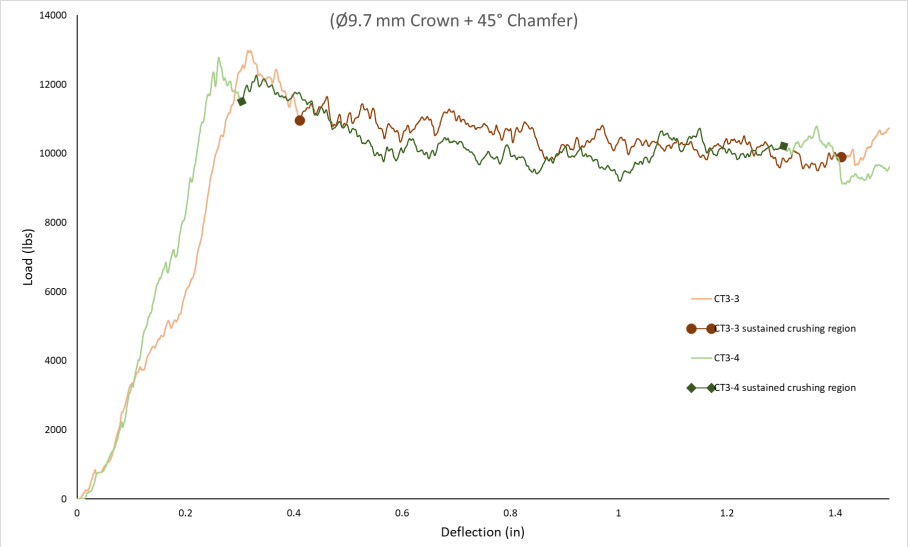

Figure 3.11: Load vs. Displacement curves for samples CT3-3 and CT3-4

3.4 Perforated Trigger (PT)

The perforated trigger is made of eight evenly spaced holes drilled into the tube wall (Figure 2.1). The purpose of the perforated trigger is to introduce stress concentrations in the tube wall at some fixed length below the loaded edge, while the edge is being crushed. This would aid in the process of formation of lateral and axial cracks for progressive crushing. PT1-1 was tested with eight 4.7mm diameter crowns on the loaded end to initiate damage, in addition to two evenly spaced rows of 4.7 mm diameter holes, with each row 12.7mm (0.5 in) apart (Figure 2.1). As seen in Figure 3.12, PT1-1 experiences an initial triggering load spike at about 6250 lbs. which is associated with the formation of lateral cracks with the help of the crown trigger, as discussed in the earlier section. However, this initial triggering spike is at a much lower load as compared to most other trigger types tested. This can be explained by the presence of the perforations in the tube wall, where the removal of some material weakens the column of material between the crown and the perforation aiding in premature shearing

of the tube wall. As loading continues, the tube wall begins splaying outwards with some axial crack formation as seen by the small load drop at about 0.10 in displacement. The load continues to rise until it peaks again at 0.2 in displacement after which there is a sudden load drop which continues for about 0.10 in of displacement. This load drop is associated with the formation of long cracks running along the length of the tube wall originating from the perforation below. The load then stabilizes and progressive crushing is observed in the Splaying Mode but at an average load value significantly lower than any other trigger type. This continues until another load spike is observed at about 0.85 in displacement. This is associated with the formation of additional cracks running along the tube length, origination from the perforation, and lateral cracks like with crown triggers, as the perforation will behave like a crown trigger once crushed through the radius of the hole. Following this load spike, the load continues to drop for about 0.40 in of displacement but this time at a lower value than for the first row of perforations. On further observation, once the sample was crushed halfway through the first row of perforations, a column of material between the two rows of perforations split apart and continued to splay outward while remaining perfectly intact (Figure 3.13). This shows that the second row of perforations has an adverse effect on the energy absorption capability with a very low SSCS of 49.11 kJ/kg, as this column of material does not contribute to the progressive crushing. To address this, PT1-2 was tested with only one row of perforations 0.50 in below the crown triggers. As seen in Figure 3.12, the initial response is similar to PT1-1 up to 0.60 in displacement. At this point, the load rises significantly and the perforation behaves like a crown trigger again. Further loading leads to stable progressive crushing until another load drop at about 1.10 in displacement which is associated with the propagation of the long cracks running along the length of the tube. To gauge the effect of the crowns on the perforated trigger, sample PT1-3 was tested with no crowns and only one row of perforations 0.50

in from the end. When loaded, the sample experienced an instantaneous large load spike up to 16000 lbs. at which point the load was sufficient to cause the tube wall to buckle and catastrophically fail, due to the weakening of the wall around a radial line running through the middle of the perforations. This shows the significance of the crown triggers in initiating the damage for progressive crushing. PT1-2 has a higher SSCS of 60.58 kJ/kg as compared to 49.11 kJ/kg for PT1-1, but still much lower than most other trigger types. Overall, results show that the tested perforated trigger types enable progressive crushing of the coupons in the splaying mode but with large load spikes at deflection values corresponding to the distance of the perforation. PT1-2 with one row of perforations shows a better energy absorbing capability at higher sustained crushing load values, as compared to PT1-1 with 2 rows of perforations.

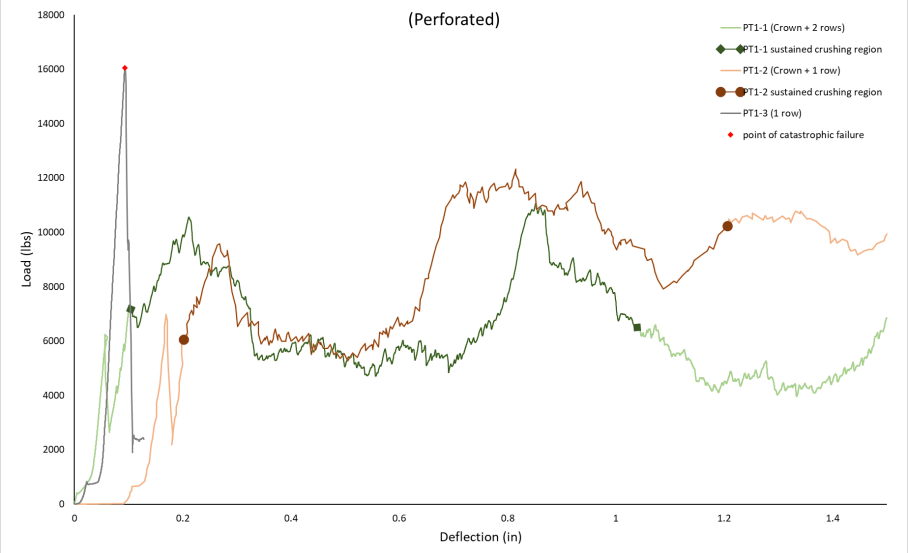

Figure 3.12: Load vs. Displacement curves for samples PT1-1, PT1-2 and PT1-3

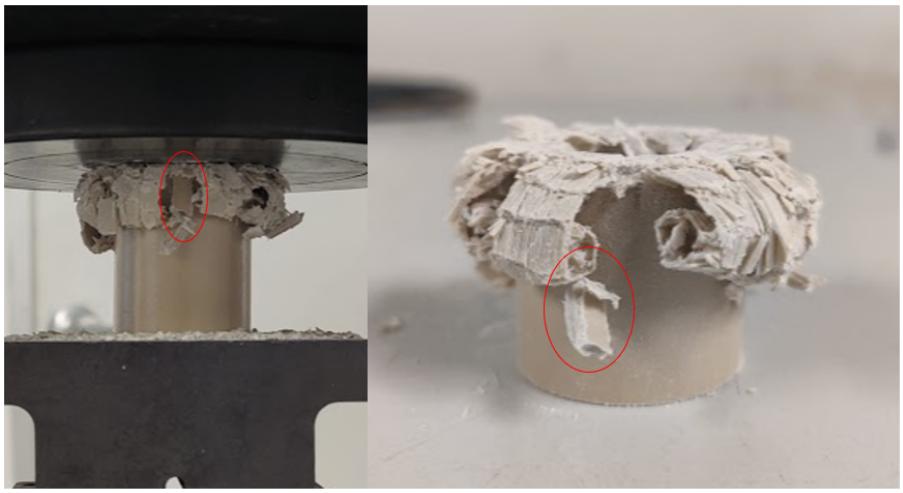

Figure 3.13: Column of intact material between rows of perforations

3.5 Effect of triggering on peak load

Figure 3.14 shows the force vs. displacement curves for four sample types, without a trigger, a 45° chamfer trigger, a 4.7 mm crown trigger and a combination of a 4.7 mm crown trigger with a chamfer. As seen, the sample without a trigger experienced a large load spike, about three times larger than the samples with triggers. In the instance of a crash, this large load value can prove fatal to the occupants of the vehicle. The purpose of an effective absorber is to reduce this initial peak load within limits that human bodies are capable of experiencing. It is clearly visible that incorporating triggers on the end of energy absorbers helps significantly reduce this initial load. A simple 45° chamfer on the end of the tube helped reduce the initial load spike by about 66%, in addition to initiating stable progressive failure. The crown trigger also helped reduce the initial load by about 71%, but with sharp load drops following the initial spike. The third trigger type shown is a combination of a crown trigger with an external chamfer. Even though this trigger type experienced a slightly higher initial load as compared to the crown trigger and chamfer trigger by themselves, it is overall more effective in

maintaining stable progressive crushing.

Figure 3.14: Comparing effect of triggerining on peak load

3.6 Effect of triggering on stable progressive crushing

When a sample without a trigger was loaded in axial compression, it experienced catastrophic failure due to shearing and buckling of fibers in the tube wall. As seen in Figure 3.15 a.), the sample without the trigger clearly shows a shear failure in the 45° plane along with some axial cracks originating from the main shear failure line. In comparison, Figure 3.15 b.) shows how the trigger helped initiate progressive failure in the splaying mode by splitting the tube wall into two sections. When initially loaded, long axial cracks are visible originating from the triggers running down the tube. This corresponds to the characteristic first load spikes visible in the load vs. displacement

curves. These axial cracks cause the tube wall to begin splitting into multiple columns or fronds, as shown in Figure 3.16 a.). As loading continues, the material under the loading platen gets pulverized and forms a wedge of debris as seen in Figure 3.16 b.). This debris wedge initiates a major central wall crack that splits the tube wall into two sections. This crack formation corresponds to the large load drop observed in the load vs. displacement curves. As seen in the figure, this debris wedge continues to split the tube wall down the middle and causes the formation of bundles of fibers that continue to splay outward. As these fiber bundles move away from the tube wall, they eventually buckle and then fold inward. This simultaneous shearing and buckling of fiber bundles continues for an extended displacement and is what contributes to the stable progressive crushing. As seen in Figure 3.17 a.), the fiber bundles splay outward and then curl inwards forming petals around the tube. Figure 3.17 b.) shows an upside-down view of the sample to display the compaction of all fronds splaying inwards. Finally, Figure 3.18 shows the observed stages of progressive crushing with the use of triggers, to better visualize the damage progression.

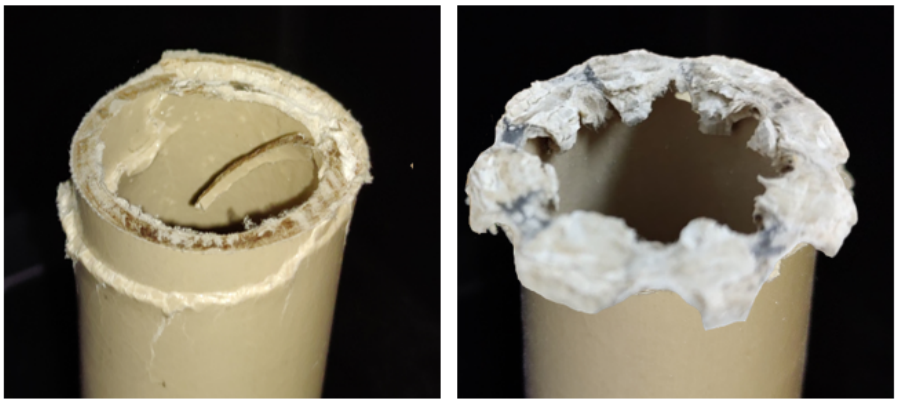

Figure 3.15: Effect of triggering on initial damage response

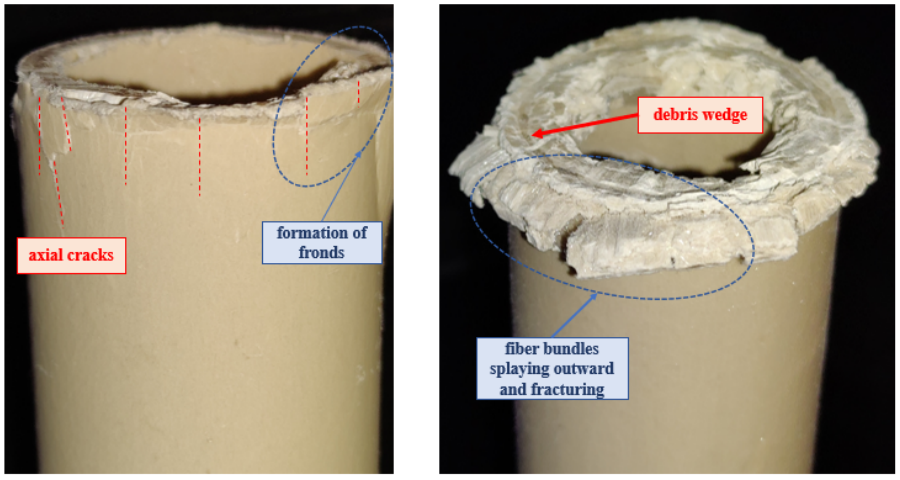

Figure 3.16: Initial response to triggering

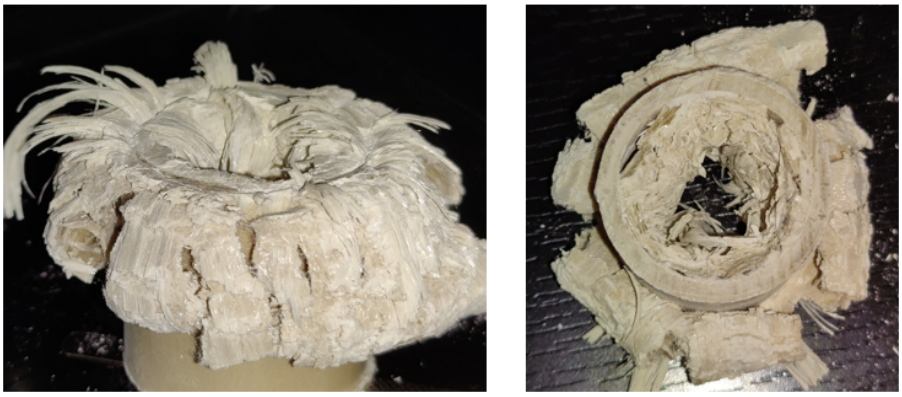

Figure 3.17: Stable damage progression in splaying mode

3.7 Effect of number of holes on energy absorption capability

Four samples with 1.5 mm diameter crowns were tested, CT1-1 and CT1-2 with 8 crowns, and CT1-3 and CT1-4 with 16 crowns. Figure 3.19 shows the load vs. displacement curves for the four samples. As seen, CT1-1 and CT1-2 have a higher

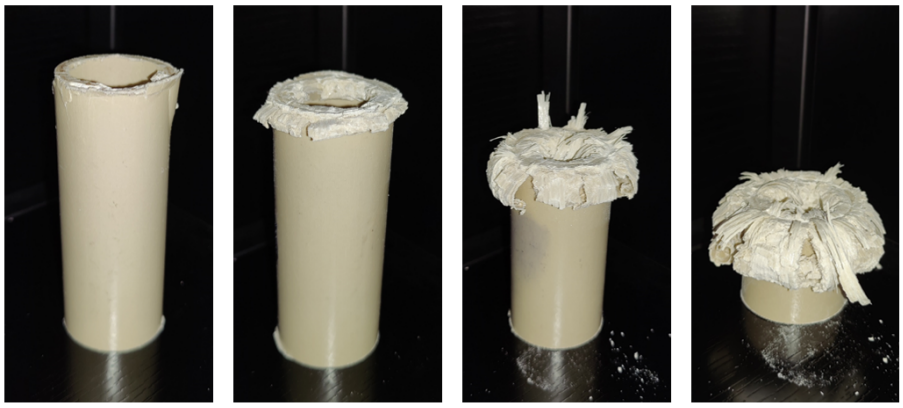

Figure 3.18: Stages of progressive crushing

sustained crushing load as compared to CT1-4. Additionally, CT1-4 shows a much larger load drop after the initial triggering phase. This implies that increasing the number of holes compromises the structural integrity of the tube wall due to which the tube continues to crush at a lower load as compared to the tubes with half the number of holes. As seen in Table 3.1 and Figure 3.20, CT1-4 has about 7% lower SSCS and about 7% lower average crushing load than CT1-2. Hence, results indicate that increasing the number of holes has an adverse effect on the energy absorption capability of tubes with crown triggers.

3.8 Effect of trigger diameter on energy absorption capability

Figure 3.21 compares the load vs. displacement curves of samples CT2-1 and CT2-2 with 4.76 mm crowns with samples CT3-1 and CT3-2 with larger 9.70 mm crowns. Results show that samples with larger diameter crowns have better energy absorption capability than samples with small diameter crowns. As seen from Figure 3.21, there is a noticeable difference in the sustained crushing load value as compared to the

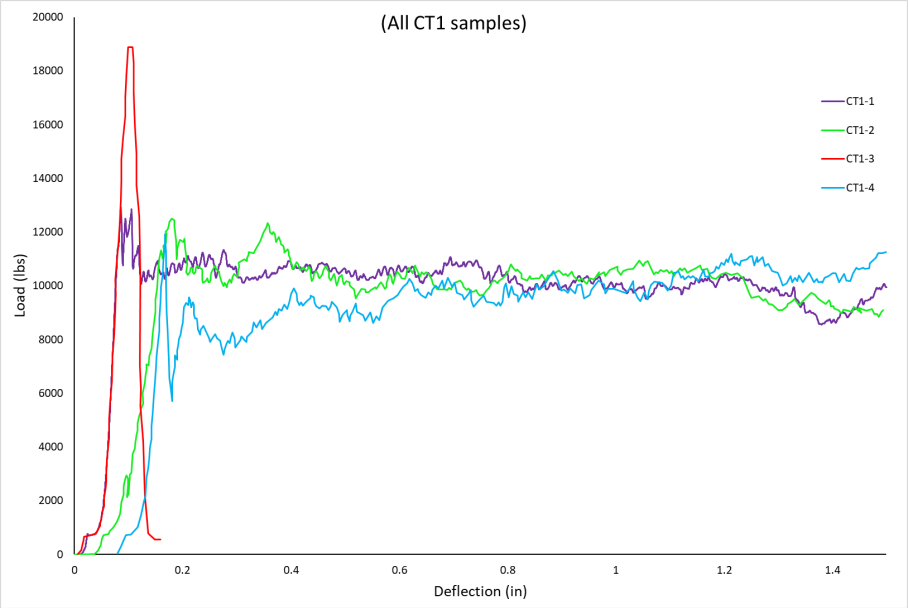

Figure 3.19: Comparing effect of numer of holes on energy absoption

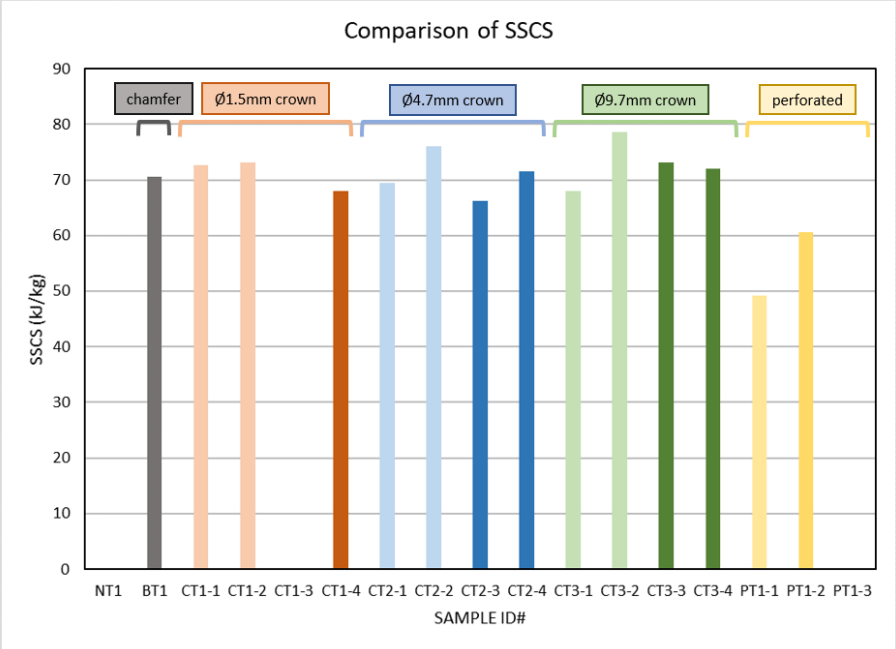

Figure 3.20: Bar chart comparing SSCS values for all samples

maximum triggering value. The larger diameter crown trigger samples experience the initial load spike at a load value slightly higher than that for the smaller diameters.

This can be attributed to the effect of the radius of curvature of the trigger hole. For a larger diameter hole with a larger radius of curvature, a greater load is required to initiate a crack as compared to a hole with a smaller diameter that has a smaller radius of curvature. The axial crack formation discussed earlier is assisted by the use of smaller diameter holes. However, this comes at a cost of energy absorption. As seen in Figure 3.20, samples with smaller diameter holes have about 3% lower SSCS than samples with larger diameter holes.

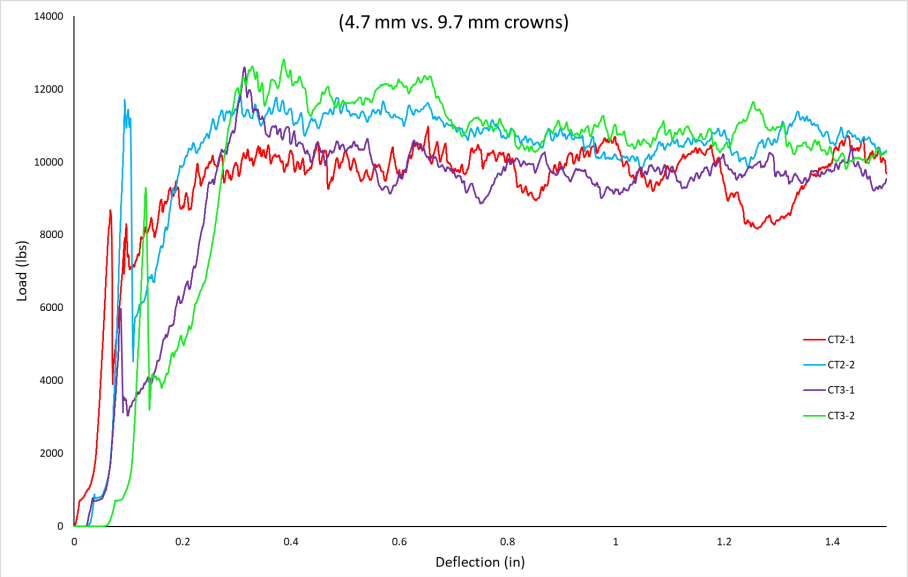

Figure 3.21: Comparing effect of crown trigger diameter on energy absorption

To address the large load drops observed for crown triggers, after the initial triggering phase, additional samples were tested incorporating a chamfer in addition to the crowns. As clearly seen in Figure 3.22 which displays the load vs. displacement curves for samples with a crown trigger and a chamfer, the samples with larger diameter crowns had a much better overall crush response. The initial load spiked at a higher value as compared to smaller diameter crowns, but remained relatively stable over an extended displacement. CT3-3 with a larger diameter crown has about 10%

higher SSCS as compared to sample CT2-3 with a smaller diameter crown. Finally, comparing the responses of all crown trigger samples, a conclusion can be drawn that the most effective crown trigger type in terms of energy absorption and efficiency in terms of triggering response would be a crown trigger with an external 45° chamfer with a diameter ranging from 5mm to 10mm.

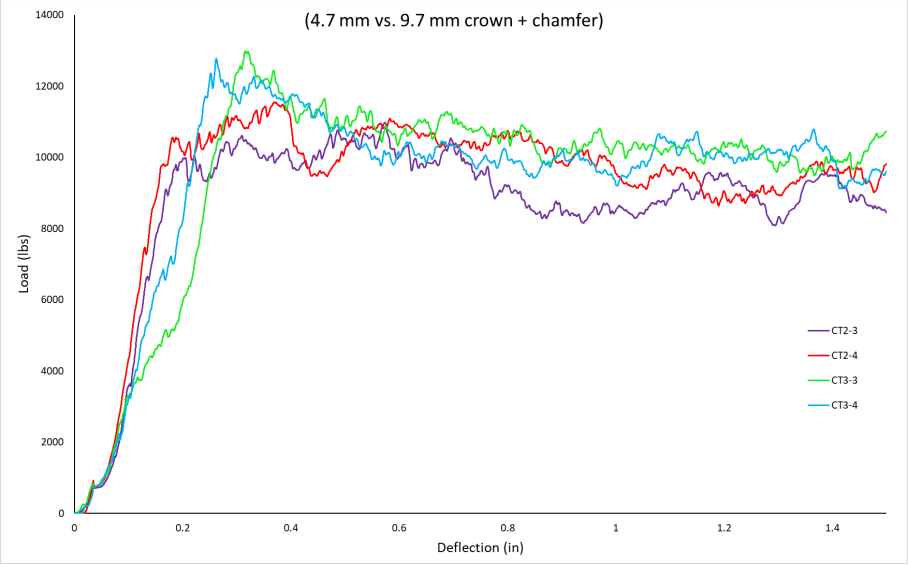

Figure 3.22: Comparing effect of chamfer+crown trigger diameter on energy absorption

Chapter 4

Conclusions

All specimens with triggers expressed stable progressive crushing in the Splaying Mode, except samples CT1-3 and PT1-2, which suffered a catastrophic failure. Both the chamfer trigger and the crown triggers are effective in reducing the peak load experienced and inducing progressive crushing. A combination of the crowns and an external chamfer performed the best of all trigger types because of the ability of the chamfer to induce damage that helps maintain the load during sustained crushing. The highest SSCS value was recorded for sample CT3-2 with eight 9.7 mm diameter crowns on one end. However, the significant load drop after triggering does not make this a favorable option. In terms of triggering response, samples CT2-3 and CT2-4 performed the best with TR values close to unity. Increasing the number of triggers was found to have no significant effect on the energy absorption capability or the crushing response. The perforated trigger helps initiate cracks in the tube wall prematurely and helps maintain progressive crushing but has poor energy absorption capability.

Overall, results of this study show that an energy absorber crown trigger with a diameter ranging from 5 to 10 mm in addition to an external 45°chamfer may be the most effective configuration in reducing the initial load experienced during a high

impact crash and efficient in maintaining progressive crushing of the absorber for pultruded energy absorbing tubes similar to those studied.

Future work can include testing additional samples of each trigger type to verify repeatability and for a larger statistical dataset. Additional material variables such as fiber type, fiber orientation and matrix type can also be introduced to study their effect on the energy absorption capability. Further testing can be conducted at increasing load rates, to compare the effects of quasi-static vs. dynamic loading on the crush response and energy absorption capability. This can be backed by developing sophisticated Finite Element (FE) models of impact loading using different trigger types. In regards to the perforated trigger, further testing can be conducted with smaller diameter perforations placed closer together to observe the difference in the crushing response.

Bibliography

[1] Florent Pled, Wenyi Yan, and Cui'e Wen. Crushing Modes of Aluminium Tubes under Axial Compression. In *5th Australasian Congress on Applied Mechanics, ACAM 2007*, pages 178–183, Brisbane, Australia, December 2007.

[2] Gary L. Farley. Energy Absorption of Composite Materials. *Journal of Composite Materials*, 17(3):267–279, May 1983.

[3] Sivakumar Palanivelu, Wim V. Paepegem, Joris Degrieck, and John Vantomme. Crushing and energy absorption performance of different geometrical shapes of small-scale glass/polyester composite tubes under quasi-static loading conditions. *Composite Structures*, 93(2):992–1007, January 2011.

[4] David C. Fleming and Karen E. Jackson. *Crashworthy Composite Structures: Aircraft & Vehicle Applications*. DEStech Publications, Inc., October 2020.

[5] Jiancheng Huang and Xinwei Wang. On a new crush trigger for energy absorption of composite tubes. *International Journal of Crashworthiness*, 15(6):625–634, 2010.

[6] Gary L. Farley. Relationship between mechanical-property and energy-absorption trends for composite tubes, 1992.

[7] D. Hull. A unified approach to progressive crushing of fibre-reinforced composite tubes. *Composites Science and Technology*, 40(4):377–421, 1991.

[8] H. Ahmad, A. A. Markina, M. V. Porotnikov, and F. Ahmad. A review of carbon fiber materials in automotive industry. *IOP Conf. Series: Materials Science and Engineering*, 971:032011, 2020.

[9] Donald F. Adams and A. K. Miller. The influence of transverse shear on the static flexure and Charpy impact response of hybrid composite materials. *Journal of materials science*, 11(9):1697–1710, 1976.

[10] S.K. Gaggar and L.J. Broutman. Strength and fracture properties of random fibre polyester composites. *Fibre Science and Technology*, 9(3):205–224, July 1976.

[11] W.R. Hoover. Crack Initiation in B-Al Composites. *Journal of Composite Materials*, 10(2):106–117, April 1976.

[12] Peter H. Thornton. Energy Absorption in Composite Structures. *Journal of Composite Materials*, 13(3):247–262, July 1979.

[13] Chiara Bisagni. Experimental investigation of the collapse modes and energy absorption characteristics of composite tubes. *International Journal of Crashworthiness*, 14(4):365–378, July 2009.

[14] A.O. Bolukbasi and D.H. Laananen. Energy absorption in composite stiffeners. *Composites*, 26(4):291–301, April 1995.

[15] J. J. Carruthers, A. P. Kettle, and A. M. Robinson. Energy Absorption Capability and Crashworthiness of Composite Material Structures: A Review. *Applied Mechanics Reviews*, 51(10):635–649, October 1998.

[16] Paolo Feraboli, Bonnie Wade, Francesco Deleo, and M. Rassaian. Crush energy absorption of composite channel section specimens. *Composites Part A: Applied Science and Manufacturing*, 40(8):1248–1256, August 2009.

[17] S. Heimbs, F. Strobl, P. Middendorf, and J. M. Guimard. Composite Crash Absorber for Aircraft Fuselage Applications. Tallinn, Estonia, July 2010.

[18] Yuen-Sheng Chiu and Syh-Tsang Jenq. Crushing behavior of metallic thin-wall tubes with triggering mechanisms due to quasi-static axial compression. *Journal of the Chinese Institute of Engineers*, 37(4):469–478, July 2013.

[19] X. Huang, G. Lu, and T. X. Yu. Collapse of square metal tubes in splitting and curling mode. *Proceedings of the Institution of Mechanical Engineers, Part C: Journal of Mechanical Engineering Science*, 220:1–13, January 2006.

[20] Michael J. Czaplicki, Richard E. Robertson, and Peter H. Thornton. Comparison of bevel and tulip triggered pultruded tubes for energy absorption. *Composites Science and Technology*, 40(1):31–46, 1991.

[21] Sivakumar Palanivelu, Wim V. Paepegem, Joris Degrieck, Johan V. Ackeren, Dimitrios Kakogiannis, Danny V. Hemelrijck, Jan Wastiels, and John Vantomme. Experimental study on the axial crushing behaviour of pultruded composite tubes. *Polymer Testing*, 29(2):224–234, April 2010.

[22] I. Sigalas, M. Kumosa, and D. Hull. Trigger mechanisms in energy-absorbing glass cloth/epoxy tubes. *Composites Science and Technology*, 40(3):265–287, 1991.

[23] Hong-Wei Song, Xing-Wen Du, and Gui-Fan Zhao. Energy Absorption Behavior of Double-Chamfer Triggered Glass/Epoxy Circular Tubes. *Journal of Composite Materials*, 36(18):2183–2198, September 2002.

[24] Peter H. Thornton and P.J. Edwards. Energy Absorption in Composite Tubes. *Journal of Composite Materials*, 16(6):521–545, November 1982.

[25] Yuqiu Yang, Asami Nakai, and Hiroyuki Hamada. Effect of collapse trigger mechanism on the energy absorption capability of FRP tubes. Kyoto, Japan, 2007.

[26] Omar Alhyari and Golam Newaz. Energy Absorption in Carbon Fiber Composites with Holes under Quasi-Static Loading. *C – Journal of Carbon Research*, 7(1):16, February 2021.

[27] Marc Courteau. Investigating the crashworthiness characteristics of carbon fiber/epoxy tubes. Master's thesis, The University of Utah, Salt Lake City, Utah, 2011.

[28] Jian-Cheng Huang and Xin-Wei Wang. Effect of the SMA Trigger on the Energy Absorption Characteristics of CFRP Circular Tubes. *Journal of Composite Materials*, 44(5):639–651, 2010.

[29] A.G Mamalis, D.E. Manolakos, M.B. Ioannidis, and D.P. Papapostolou. On the response of thin-walled CFRP composite tubular components subjected to static and dynamic axial compressive loading: Experimental. *Composite Structures*, 69(4):407–420, August 2005.

[30] Deepak Siromani, Gary Henderson, Doug Mikita, Kevin Mirarchi, Ryan Park, John Smolko, Jonathan Awerbuch, and Tein-Min Tan. An experimental study on the effect of failure trigger mechanisms on the energy absorption capability of CFRP tubes under axial compression. *Composites Part A: Applied Science and Manufacturing*, 64:25–35, September 2014.

[31] Scott E. Stapleton and Daniel O. Adams. Crush Initiators for Increased Energy Absorption in Composite Sandwich Structures. *Journal of Sandwich Structures and Materials*, 10(4):331–354, July 2008.

[32] Yan Tong, Yuanming Xu, Jidong Wang, and Bajracharya Suman. Energy absorption capability of carbon fiber reinforced plastic tubes with semi-circle grooved external trigger. *Journal of Reinforced Plastics and Composites*, 35(20):1460–1476, 2016.

[33] Rubentheran Sivagurunathan, Saijod L. T. Way, Linkesvaran Sivagurunathan, and Mohd Y. Yaakob. Effects of triggering mechanisms on the crashworthiness characteristics of square woven jute/epoxy composite tubes. *Journal of Reinforced Plastics and Composites*, 37(12):824–840, 2018.

[34] A.A.S Abosbaia, E. Mahdi, A.M.S Hamouda, and B.B Sahari. Quasi-static axial crushing of segmented and non-segmented composite tubes. *Composite Structures*, 60(3):327–343, 2003.

[35] Bruno Goncalves Coghi, Dante K. De'Grandis, and David C. Fleming. Analysis of the Crushing of Metal/Composite Tubes Under Compressive Load. In *Proceedings of the 2017 SAMPE Conference*, Seattle, WA., May 2017.

[36] S. S. A. Lykakos, P. K. Kostazos, O. Venetsanos, and D.E. Manolakos. Crashworthiness Performance of Aluminium, GFRP and Hybrid Aluminium/GFRP Circular Tubes under Quasi-Static and Dynamic Axial Loading Conditions: A Comparative Experimental Study. *Dynamics*, 1(1):22–48, 2021.

[37] H. R. Zarei. Experimental and numerical crashworthiness investigationof hybrid composite aluminum tubes under dynamic axialand oblique loadings. *International Journal of Automotive Engineering*, 5(3):1084–1093, September 2015.

[38] F. C. Bardi, H. D. Yun, and S. Kyriakides. On the axisymmetric progressive crushing of circular tubes under axial compression. *International Journal of Solids and Structures*, 40:3137–3155, June 2003.

[39] Gary L. Farley. *Energy-absorption capability of composite tubes and beams*. Ph.D. Thesis, Virginia Polytechnic Institute and State University, Blacksburg, Virginia, May 1989.

[40] V. Kostopoulos, Y. P. Markopoulos, D. E. Vlachos, C. Galiotis, and N. E. Melanitis. A heavy duty composite bridge made of glass/polyester pultruded box beams. In *Proceedings of the 10th European Conference on Composite Materials: Composites for the Future*, volume 8, Brugge, Belgium, January 2002.

[41] H. Luo, Y. Yan, X. Meng, and C. Jin. Progressive failure analysis and energy-absorbing experiment of composite tubes under axial dynamic impact. *Composites Part B: Engineering*, 87:1–11, February 2016.

[42] A.G Mamalis, M. Robinson, D.E. Manolakos, G.A. Demosthenous, M.B. Ioannidis, and J. Carruthers. Crashworthy capability of composite material structures. *Composite Structures*, 37(2):109–134, 1997.

[43] J. Michael Starbuck, Daniel O. Adams, and Marc Courteau. Energy Absorbing Damage Mechanisms in Progressive Crushing of Composite Tubes. In *Proceedings of the American Society for Composites 32nd Technical Conference*, West Lafayette, Indiana, USA, October 2017.

[44] Gary L. Farley and Robert M. Jones. Crushing Characteristics of Continuous Fiber-Reinforced Composite Tube. *Journal of Composite Materials*, 26(1):37–50, January 1992.

[45] A.G Mamalis, D.E. Manolakos, G.A. Demosthenous, and M.B. Ioannidis. The static and dynamic axial collapse of fibreglass composite automotive frame rails. *Composite Structures*, 34(1):77–90, 1996.

[46] Peter H. Thornton. The Crush Behavior of Pultruded Tubes at High Strain Rates. *Journal of Composite Materials*, 24(6):594–615, June 1990.

[47] Damien Guillon, Samuel Rivallant, Jean-Jacques Barrau, Caroline Petiot, Pascal Thévenet, and Nicolas Pechnik. Initiation and propagation mechanisms of progressive crushing in carbon-epoxy laminated plates. Stockholm, Sweden, June 2008.

[48] Norman Jones. *Structural Impact*. Cambridge University Press, 2 edition, June 2012.

Appendix

All the results tables and plots presented in this paper are present in this Appendix.

Table A.1: Summary of results

Specimen ID	SSCS (kJ/kg)	SSCS (kip_f in/lb_m)	TR	P_{max} (kip)	P_m (kip)
NT1	-	-	-	29.81	-
BT1	70.69	283.75	1.01	10.23	10.11
CT1-1	72.63	291.54	1.24	12.92	10.39
CT1-2	73.13	293.53	1.19	12.50	10.46
CT1-3	-	-	-	18.90	-
CT1-4	68.07	273.21	1.22	11.89	9.74
CT2-1	69.43	278.68	0.87	8.68	9.93
CT2-2	76.02	305.14	1.08	11.71	10.87
CT2-3	66.23	265.83	1.06	10.10	9.47
CT2-4	71.48	286.90	1.03	10.55	10.22
CT3-1	67.95	272.77	1.30	12.60	9.72
CT3-2	78.66	315.76	0.83	9.30	11.25
CT3-3	73.12	293.51	1.24	12.98	10.46
CT3-4	72.03	289.14	1.24	12.78	10.30
PT1-1	49.11	197.13	0.89	6.24	7.03
PT1-2	60.58	243.18	0.81	6.99	8.67
PT1-3	-	-	-	16.04	-

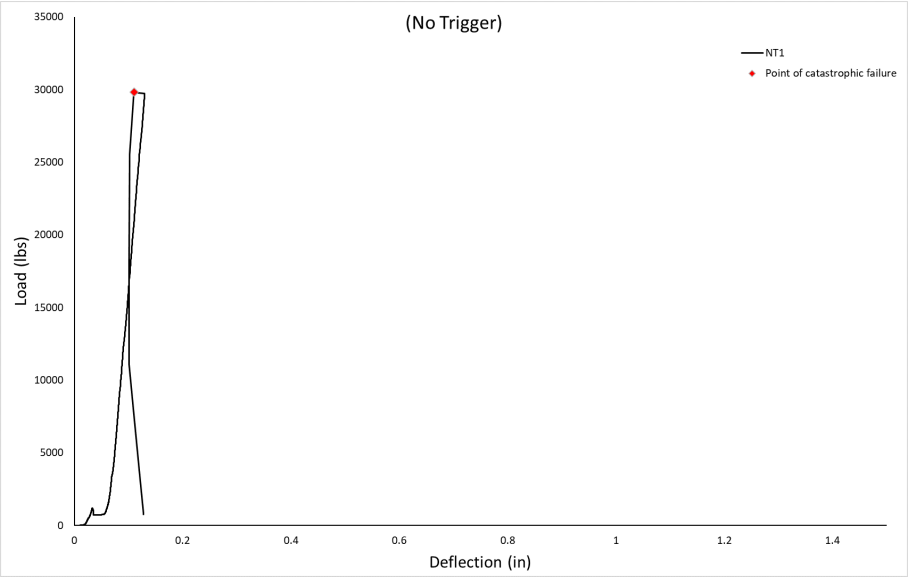

Figure A.1: Load vs. Displacement curve for sample NT1

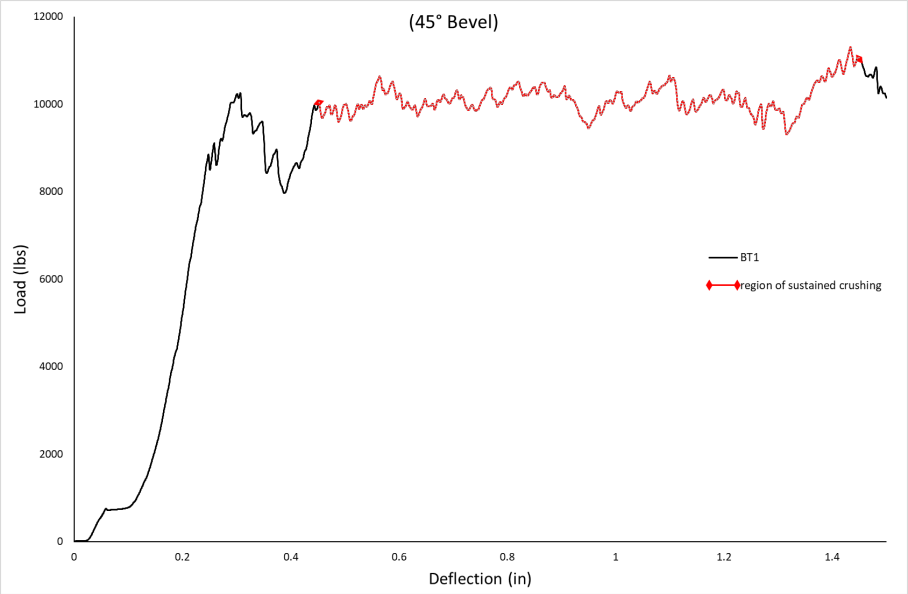

Figure A.2: Load vs. Displacement curve for sample BT1

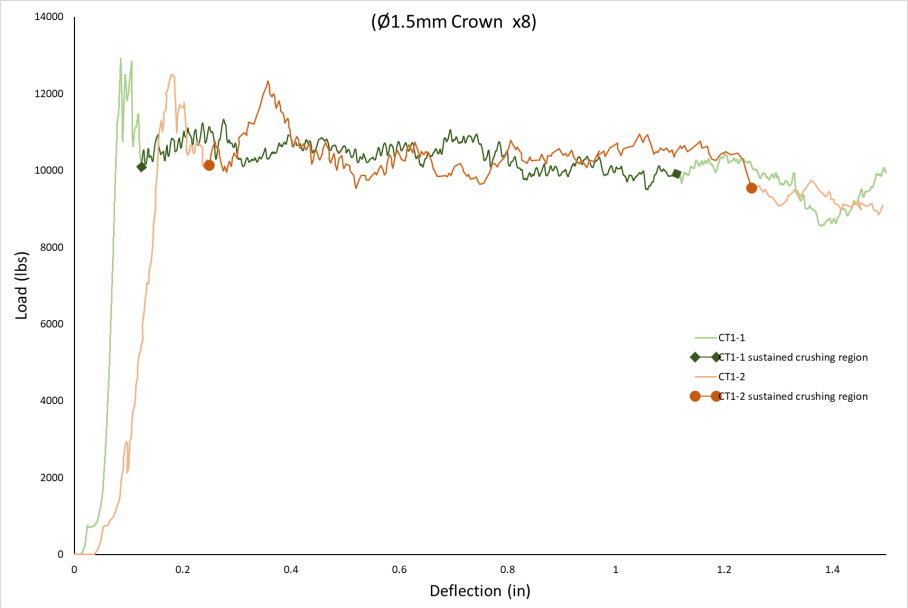

Figure A.3: Load vs. Displacement curves for samples CT1-1 and CT1-2

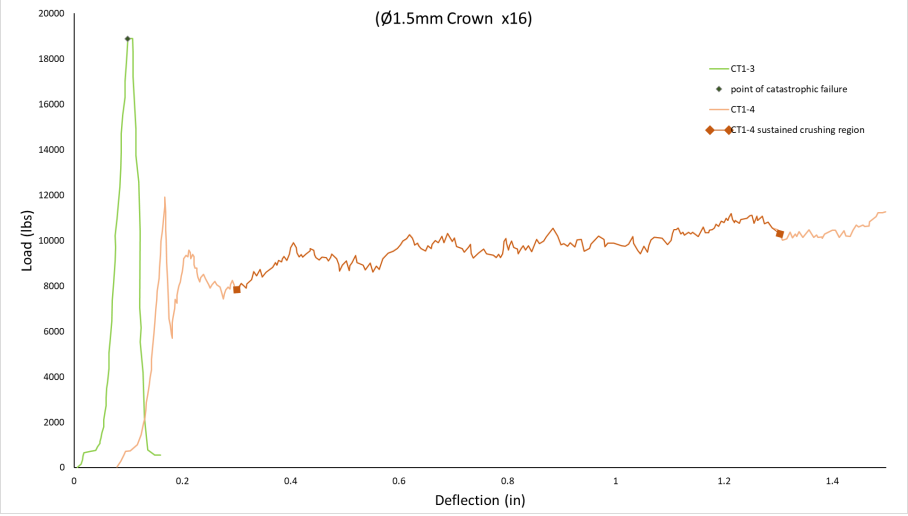

Figure A.4: Load vs. Displacement curves for samples CT1-3 and CT1-4

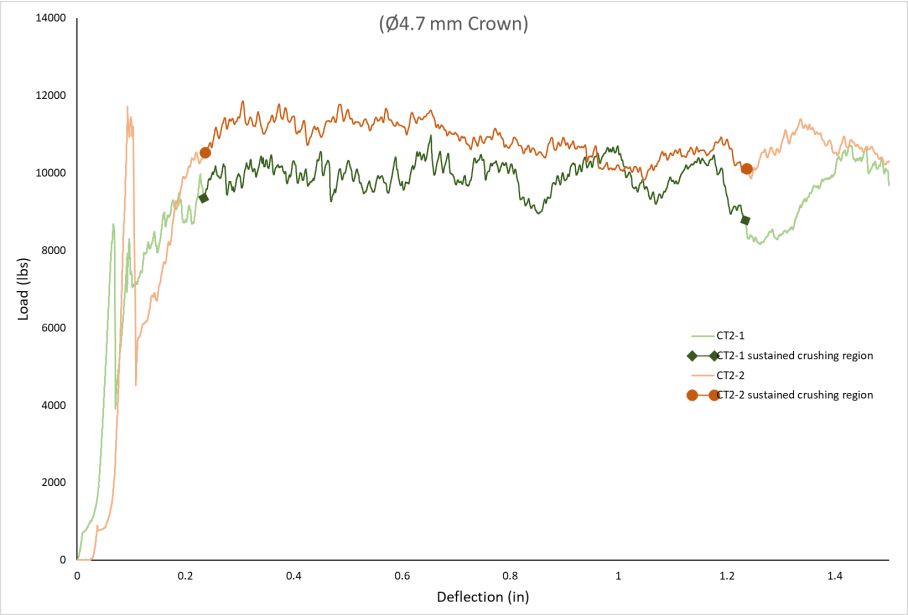

Figure A.5: Load vs. Displacement curves for samples CT2-1 and CT2-2

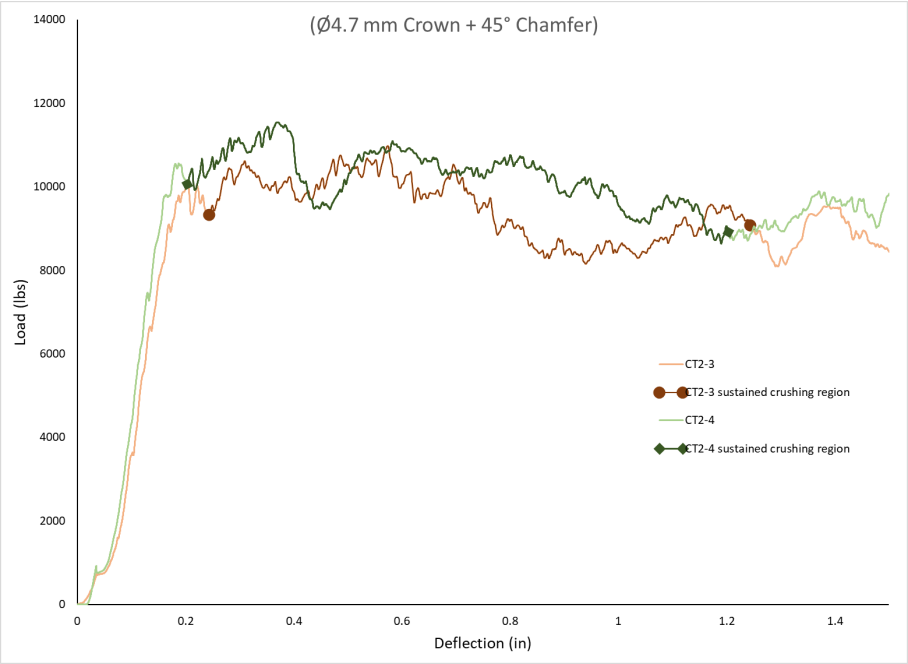

Figure A.6: Load vs. Displacement curves for samples CT2-3 and CT2-4

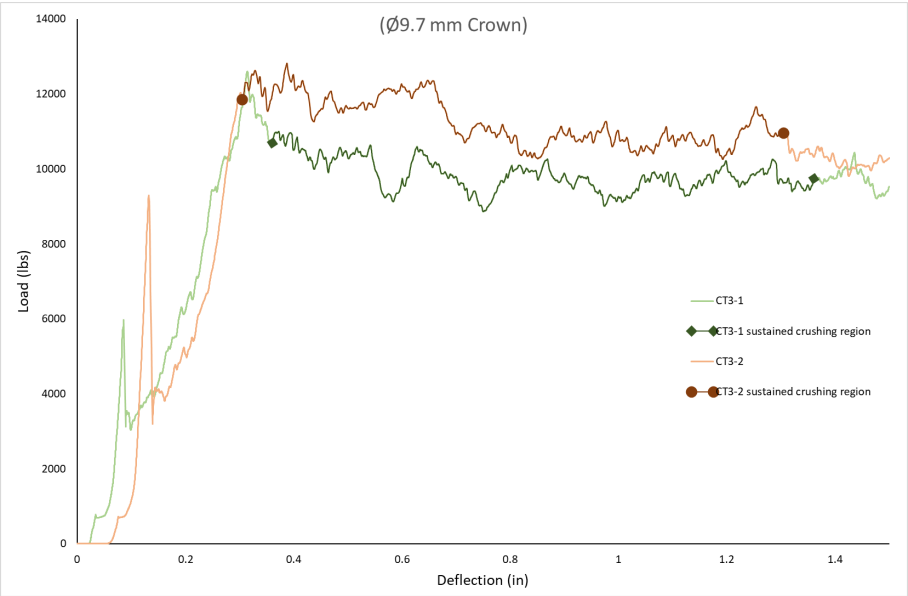

Figure A.7: Load vs. Displacement curves for samples CT3-1 and CT3-2

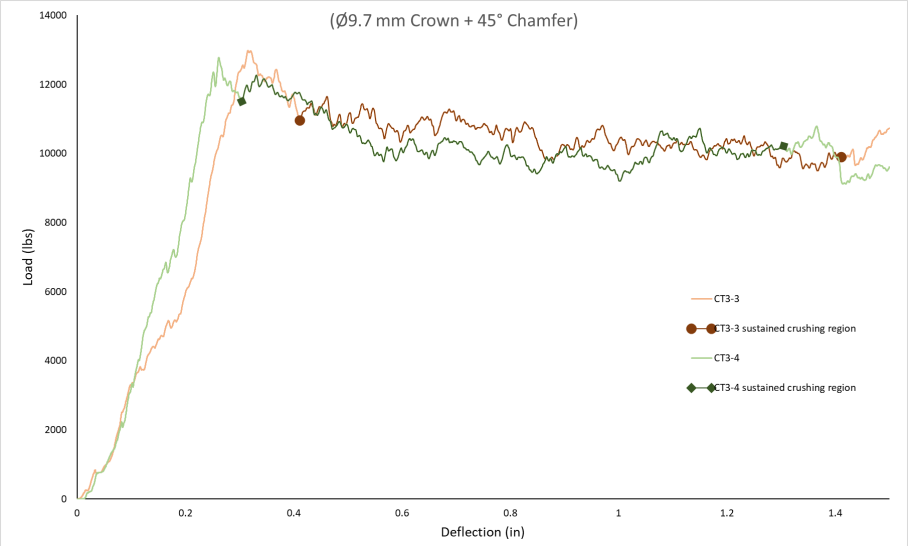

Figure A.8: Load vs. Displacement curves for samples CT3-3 and CT3-4

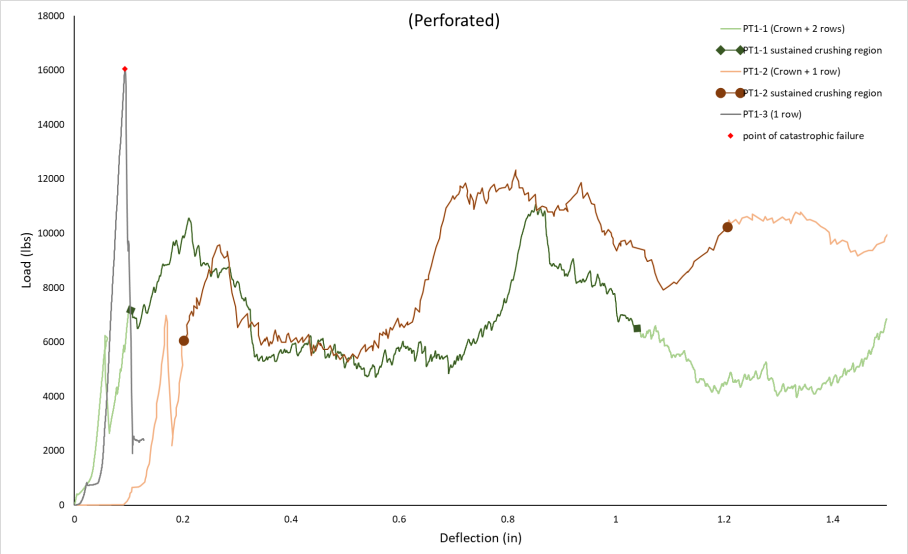

Figure A.9: Load vs. Displacement curves for samples PT1-1, PT1-2 and PT1-3

Figure A.10: Comparing effect of triggerining on peak load

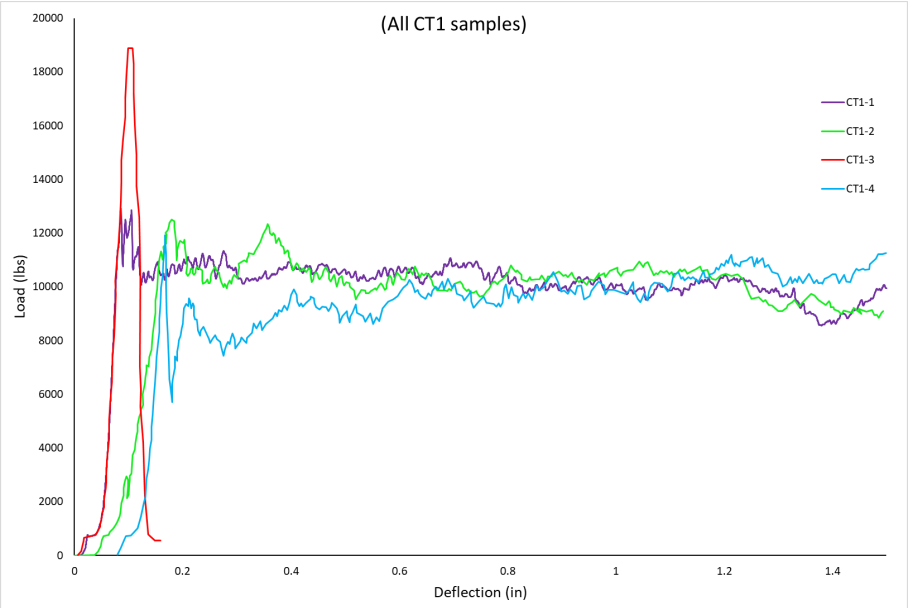

Figure A.11: Comparing effect of numer of holes on energy absoption

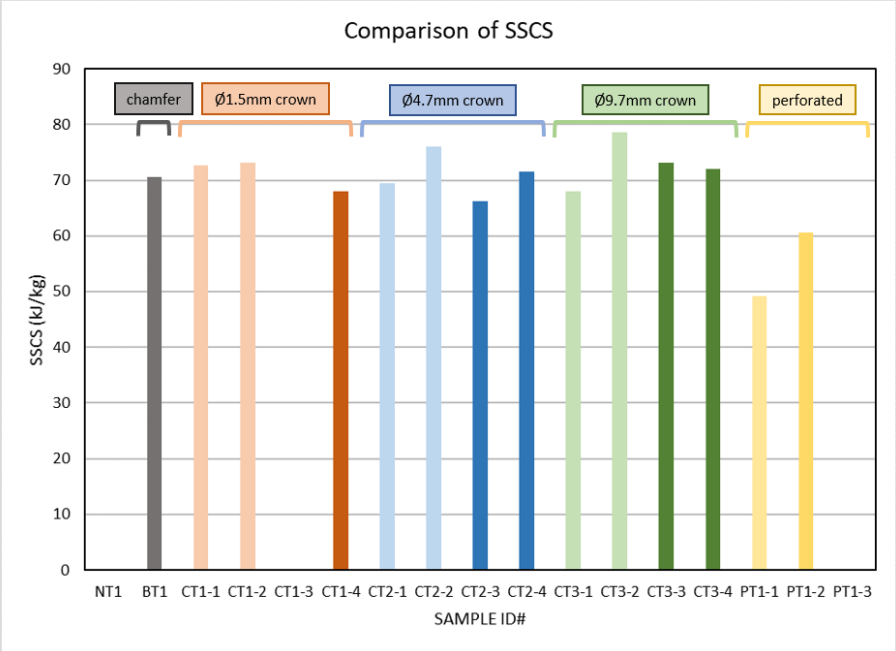

Figure A.12: Bar chart comparing SSCS values for all samples

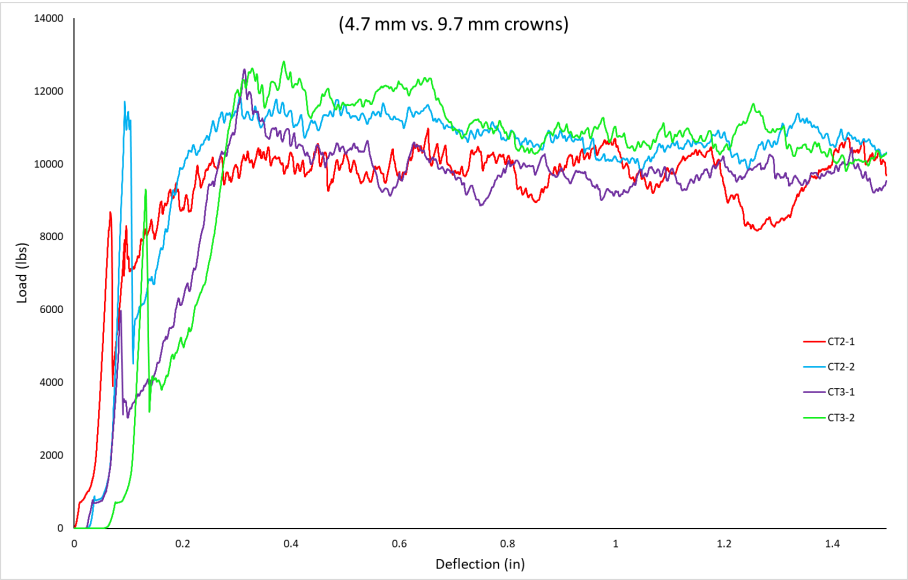

Figure A.13: Comparing effect of crown trigger diameter on energy absorption

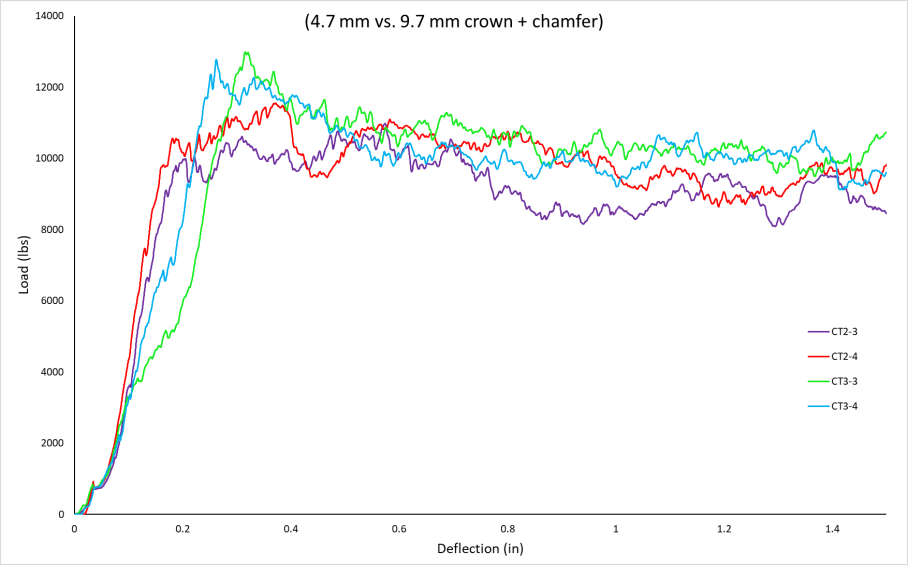

Figure A.14: Comparing effect of chamfer+crown trigger diameter on energy absorption